UNIVERSITÀ DELLA CALABRIA

UNIVERSITA' DELLA CALABRIA

Dipartimento di Chimica e Tecnologie Chimiche

Dottorato di Ricerca in

Medicina Traslazionale

CICLO

XXIX

TITOLO TESI

New non invasive conservation methods for Cultural heritage

Settore Scientifico Disciplinare

Chemistry, Materials Science, Chemistry of the Cultural Heritage

Coordinatore: Ch.mo Prof. Sebastiano Andò

Firma _____

Supervisore/Tutor: Ch.mo Prof. Giuseppe Chidichimo

Firma _____

Dottorando: Dott. Francesco Dalena

Firma _____

A Daniele.

Che il vento ti sia sempre in poppa,

cavaliere.

CONTENTS

PREFACE

This PhD work, involves the study of new methods for the conservation of Wood and membranaceous historical and artistic artifacts with respect biochemical and chemical attacks. The project wanted to face with two different aspects of the problems. From one side new methodologies had to take into account the possibility of producing restoration and conservation techniques much less invasive with respect to the historical artifacts themself. On the other hand these new methods would also preserve operators involved in practical conservative works from exposure to aggressive chemicals. Our studies will than take into account new methods for both wood works and the old books. In the course of this thesis work we had also to deal with standardization of measurements concerning book acidity (pH measurements). We have pointed out that, in order to better use pH values, new measurements procedures needed to be developed, also in concomitance with the development of a sophisticated mathematical model.

Going back to main arguments treated in this thesis, that is to say the disinfestation of wood artifacts from beds and other biologic attacks, and the de-acidification of ancient books, we wont to underline that conservation and restoration,, in these contests involve quite dangerous manipulations of chemical products. The most effective methods for the removal of wood-eating insects are those that use of methyl bromide and ethylene oxide which appear to be human carcinogens and toxic to the environment. Other techniques, less toxic, making use of the help of sealed chambers in which oxygen in the air is replaced with nitrogen treatment times are very long (about thirty days of treatment). One of the aim of this work was to develop physical low invasive treatment of historical wood, having a zero impact with health of the operator, and being almost not invasive for the artifacts. Two methodologies have been developed. One of this was the use of microwave irradiation at low heat transfer, starting from the concept that biologic parasite generally contain greater amount of water with respect to artifact materials. Thus during well calibrated irradiations with microwaves, bio-infestants should have an antenna role absorbing the main part of irradiated energy, and leaving the artifact cold. Another physical treatment which h has been found worth to explore was the use of vacuum conditions which could bring the bio-infestant quickly out of their living pressure gradients. These two physical methods appeared to be very easy applicable in the conservation and restoration practices.

The other main argument treated in tis thesis has been news methods for neutralize the acidity of the ancient book. The acidity of the paper is the main cause of degradation of the books. The cellulose while being an extremely stable polymer, it will degrade over time for both oxidizing action of oxygen and also hydrolysis in the presence of acids. The acidic hydrolysis proceeds with greater speed for the catalytic action of H^+. Moreover hemicellulose (the other form of cellulose contained in the paper), are more easily hydrolysed than cellulose.

The breakage of the polymer chains leads to the progressive deterioration of the fibers and therefore of the paper sheets. As a side effect, there is also a progressive increase in oxidation involving atmospheric oxygen, this also conditioned by acid hydrolysis. The effect of oxidation is the appearance of yellowing paper.

The optimal degree of pH of the paper is around 7.5, the card that has a pH below 5 is destined to deteriorate in a short time. The deacidification is the restoration intervention to reduce the degree of acidity of the paper, also ensuring alkaline reserve which neutralizes any new appearance of acids

The treatment can be performed in aqueous or non-aqueous environment. The wet treatment is performed by immersing the sheets in a solution obtained by adding water or the salts of basic substances, such as calcium bicarbonate and calcium hydroxide. After washing, the sheets are generally put out to dry on absorbent paper or on the vacuum table. This very invasive techimique is among the most common in the laboratories of book restoration, especially for books and archival documents, and yet, despite the undeniable positive effects, also can cause unexpected negative impact on artefacts.

A part of this research work has been focused on the consolidation of an innovative, not destructive methodology to recover ancient book acidity. In particular our efforts have been devoted to de-acidify the ancient texts by aerosol techniques, where micro-droplets of low alkaline solutions have been spread on the surface of the book pages. We will show that the technique is very rapid full effective, and not secondarily very less expensive than currently used treatments.

When measurements of the pH were carried out, a continuous drifting of the measurements detected by the contact pH meter was observed. For this reason a new measurement technique has been developed to improve the accuracy of pH measurements made by surface contact pH meter.

Part 1

New not invasive methods for wood artefact conservation

This first part of the thesis is divided into three chapters. The first chapter "*The chemistry of wood: structure and properties. A review chapter*" is a review of the physical - chemical properties of the wood and its chemical composition; particular attention is given to cellulose, the raw material of paper. This chapter gives a short reminding of some of the basic concepts useful for full understanding most of the experimental work discussed in this thesis. Chapter 2 and chapter 3 discuss the experimental work carried out on wood samples for the elimination of biological infestation. In particular, in Chapter 2, *"Insect-Infested Wood Remediation by microwave heating and its effects on wood dehydration: a case study of Hylotrupes bajulus larva"*, an innovative experimental work which dealt the elimination of biological infestations by using microwaves, it is reported. This paper reports also the possible water loss of the wood under microwaves irradiation. Chapter 3 " *Woodworm disinfestation of wooden artefacts by vacuum techniques* " reports the experimental work regarding the application of vacuum techniques to eliminate biologic infestations from wood artefacts.

Chapter 1

The chemistry of wood: structure and properties. A review chapter

For a better understanding of the work done during this PhD, the first chapter of this thesis is focused on the chemistry of the wood and its derivatives (such as cellulose).
In fact, wood is an extremely versatile material with a wide range of physical and mechanical properties among the many species of wood. It is also a renewable resource with an exceptional strength-to-weight ratio. This chapter has been divided into two parts: the chemistry of the wood and its compounds and the chemical-physical properties. Need to specify that in this chapter are not addressed all the properties of wood and cellulose, but only those which can be found interest in the understanding of the thesis work with special attention, for example on such anisotropic and hygroscopic properties of the wood.

1.1 Chemistry compounds of wood

The wood consists of olocellulose (divided into cellulose (40-50%) and hemicellulose (25-35%)) and lignin (15-20%) along with a small percentage of pectin, protein, extravtives and ash (1-15%) (Sun and Chen, 2002; Ritter, 2008; Sanderson, 2011).

Cellulose and starch
Cellulose is a linear polimer of D-glucose units linked toghether by β – (1,4) – glycosidic bond (see Figure 1.1), while cellobiose is the reaper unit of cellulose chains.

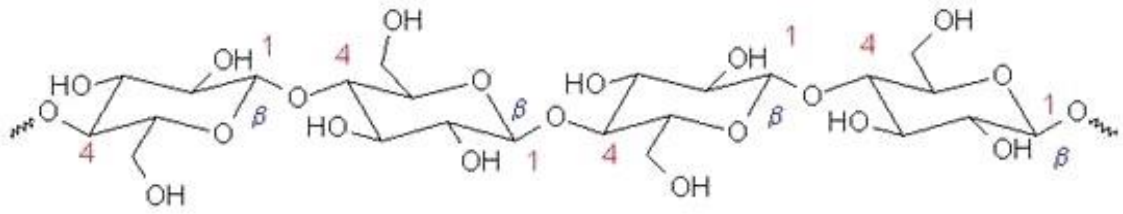

Figure 1.1. *Chemical structure of cellulose: the long chain unbrached polymers containing D-glucose units linked toghether by β – (1,4) – glycosidic bond*

Through β – (1,4) – glycosidic bond is not so difficult to break, the intense hydrogen bonding beetween the hydroxyl groups on the glucose of one chain with the oxygen atom of a same or neighboring chain provides the rigidity and high-tensile streght of microfibrils (Pettersen, 1984). The tight and well-organitation of the crystalline domains prevent the penetration of reagents like water or enzyme. Cellulose is completely insoluble in normal aqueous solutions as water is unable to penetrate through crystalline cellulose, with creates high resistance to efficient hydrolysis. While in amorphous cellulose, endogluconase (a subgroup of cellulase enzyme) can easily penetrate and catalyzesthe hydrolysis of internal bonds. Hence the hydrolysis rate of amorphous cellulose is much faster than crystalline cellulose. The transition of crystalline cellulose to amorphous one demands the temperature of 320 °C and the pressure of 25 MPa (Ververis et al., 2004).

As for the cellulose, also for the starch have several glucose units joined to form long chains. However, their roles are quite different: while the starch acts as a reserve substance, the cellulose is used as a support structure. This is understandable if you look at the different type of relationship between the glucose molecules in starch and cellulose (Fig. 1.2). In the first the different monomers are linked via α type bond, while the last of these are type β. This difference is not meaningless: the α bond is more easy to break, and its formation requires the rolling up of the chain so that the -OH groups of the starch protrude inside of the spiral, escaping to any aggregation with adjacent molecules.

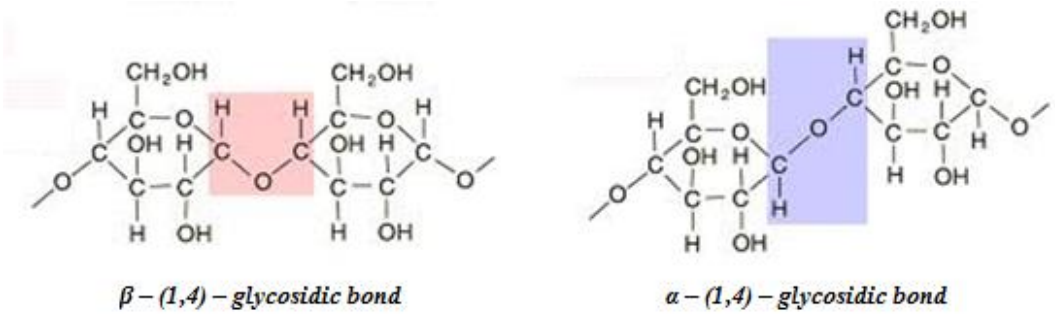

Figure 1.2. *Differences beetween bonds of glucose (β – (1,4) – glycosidic bond) and starch bond (α – (1,4) – glycosidic bond)*

Such properties are suitable to the type of starch turning function: it is packaged in the spare areas of the plant and, when needed energy, a molecule of glucose is easily detached by hydrolysis to then be readily metabolized. In opposition the binding β is more difficult to break and gives the chain a rectilinear configuration, stabilized by hydrogen bonds formed by -OH groups and which allow the aggregation of bundles of more adjacent cellulose molecules, essential characteristic to provide stability, strength and rigidity. These bundles form the central part, said crystallite, which represent the microfibrils of the wood reference unit. The microfibrils are in turn combined to form the fibrils, which together form fibers.

Hemicellulose

Hemicellulose is a low-molecolar weight amorphous polymer consisting of different monosaccharides, including pentose (xylose and arabinose), hexoses (glucose, mannose and galactose) and uronic acid substituent [i.e. 4-o-methylglucuronic acid ($C_7H_{12}O_7$), D-glucuronic acid ($C_6H_7O_7$) and D-galacturonic acid ($C_6H_{10}O_7$) as shown in Figure 1.3] (Mazumder et al., 2015; Sloneker, 1971).

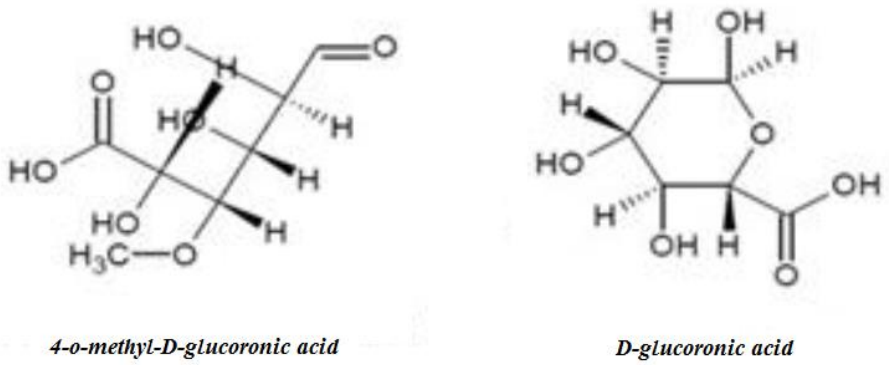

Figure 1.3. *Chemical structure of 4-o-methylglucuronic acid ($C_7H_{12}O_7$), D-glucuronic acid ($C_6H_7O_7$).*

The hemicellulose could be either a homopolymer or a heteropolymer with short lateral branches (consisting of different sugars) linked together by β – (1,4) – glycosidic bonds and sometimes by β – (1,3) – glycosidic bonds (Figure. 1.4)

These branching may be chemically linked to molecules that are not classified as hemicelluloses, for example with phenol or with the same lignin molecules via covalent bonds. With cellulose instead it binds, via hydrogen bonds, in microfibrils going to form the peripheral portion (amorphous area) of them.

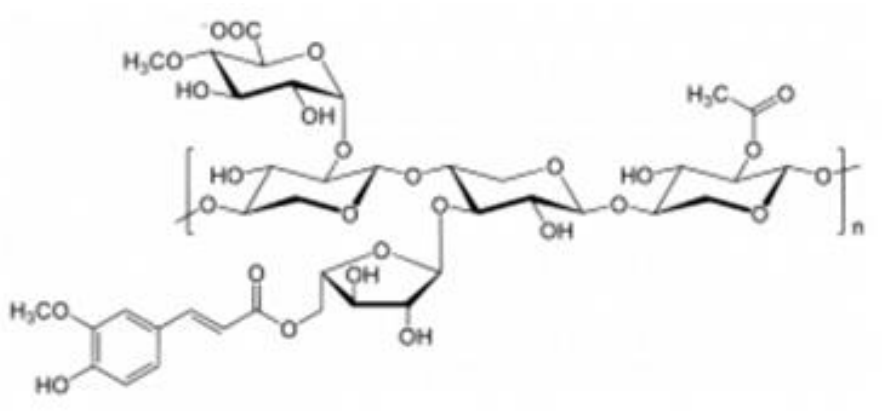

Figure 1.4. *Chemical structure of hemicellulose xilane*

Hemicellulose has fewer moduli of elasticity andhence contributes very less to the structure of the material. Contrary to cellulose, hemicellulose is relatively easy to hydrolyze into monomers (Mazumder et al., 2015; Ritter, 2008; Kumar et al., 2009; Sanderson, 2011). The main distinguishing feature between hemicellulose and cellulose is that hemicellulose is an amorphous low molecular weight branched polymer, while cellulose is a crystalline long chain linear polymer.

Lignin

Lignin is nature's most abundant aromatic polymer and hydrophobic in nature. It is a large amorphous cross-linked hetero polymer constituting of three phenyl propionic alcohol building units: coniferyl alcohol (*guaiacyl propanol*) Figure 1.5a, coumaryl alcohol (p-*hydroxyphenylpropanol*) Figure 1.5b and sinapyl alcohol (*syringyl alcohol*) Figure 1.5c

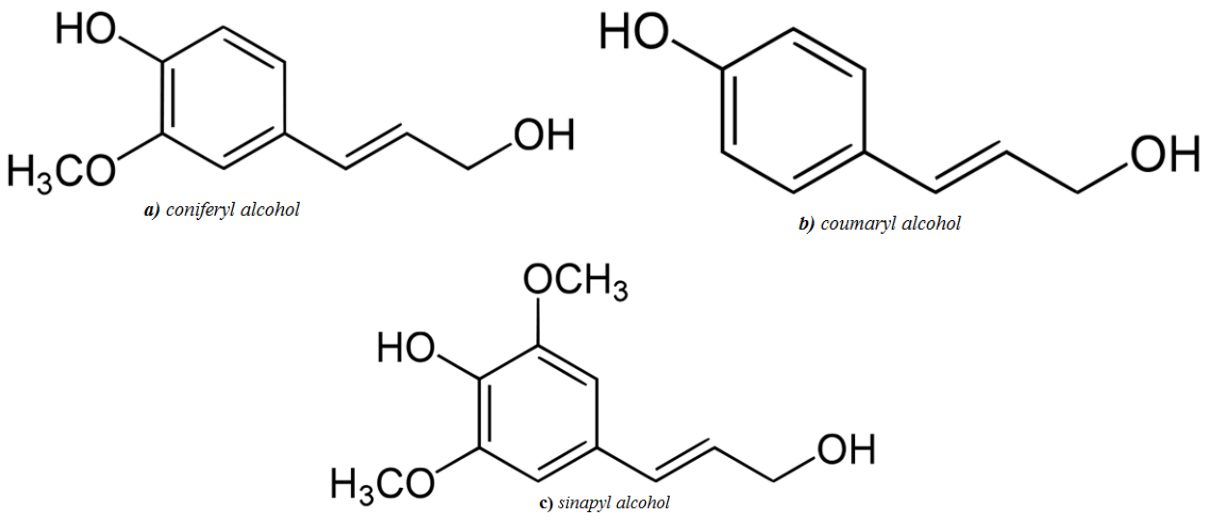

Figure 1.5. *Chemical structure of guaiacyl propanol (a), coumaryl alcohol (b) and sinapyl alcohol (c)*

These phenolic monomers are linked together by alkyl-aryl, akyl-alkyl and aryl-aryl bonds making a three-dimensional network structure (Figure 1.6). It helps to provide plants structural support, impermeability, resistance against microbial attack and oxidative stress. Hardwood contains comparatively less lignin than softwood (Taherzadeh, 2007; Kumar et al., 2009; Hendriks and Zeeman, 2009).

The lignin is responsible for the lignification of plant tissue and is distinguished in the different plant species in size and shape in relation to the type of cells in which it is present and the type of wood. Lignin is linked by ether linkages with the cellulose molecules. The current methods of extraction tend to solubilize the three monomer units (*guaiacyl propanol*, p-*hydroxyphenylpropanol* and *syringyl alcohol*) that appear to be water soluble.

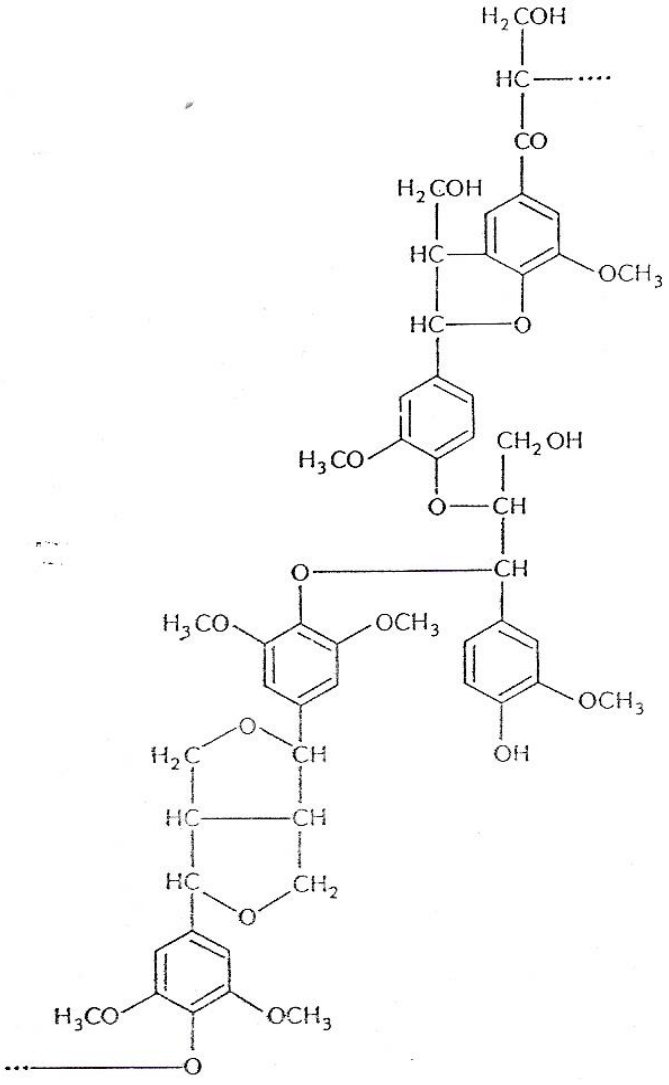

Figure 1.6. *Partial chemical structure of lignin*

Extractives

Extractives finally include various kinds of compounds such as starch and phenols. They may confer important to wood chemical-physical properties, such as: color, durability, chemical stability, etc.

A key distinction between these extractable substances, defined as a whole "extractive", can be made on the basis of their solubility in water rather than in a mixture of apolar organic solvents.

Among the most important extractable substances in water they are: polyphenols, hydroxybenzoic acids (eg. Salicylic acid extracted from willow bark) and catechins (including some in common with those known in green tea). Among the soluble extraction in organic solvents, the most common are those that become part of the so-called essential oils.

The best-known essential oils extracted from woods are probably those of sandalwood and cedarwood. The resins of conifers such as pine and fir are another class of extractives from wood soluble in organic solvents, more rich in fixed components, or non-volatile, compared with essential oils: from coniferous resin can be separated and recover its more volatile fraction, a kind of essential oil from the resin, known as turpentine and marketed under the name of turpentine (paint thinner).

1.2 Chemical – physical proprieties of wood

Wood may be described as an orthotropic material; that is, it has unique and independent mechanical properties in the directions of three mutually perpendicular axes: longitudinal, radial, and tangential. The longitudinal axis *L* is parallel to the fiber (grain); the radial axis *R* is normal to the growth rings (perpendicular to the grain in the radial direction); and the tangential axis *T* is perpendicular to the grain but tangent to the growth rings. These axes are shown in Figure 1.7 (adapted from Green et al., 1999).

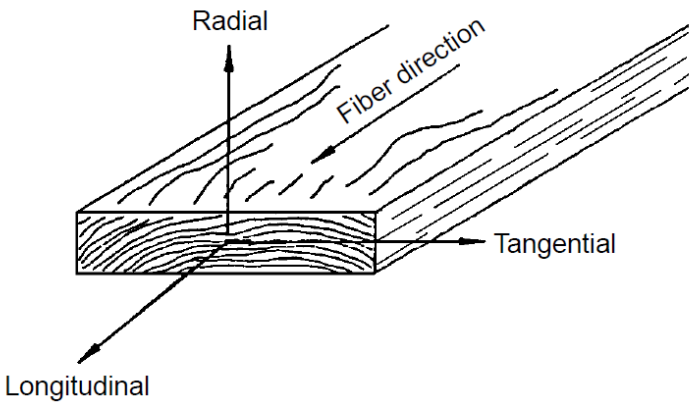

Figure 1.7. *Three principal axes of wood with respect to grain direction and growth rings*

Moisture Content

The moisture content of wood is defined as the weight of water in wood given as a percentage of oven dry weight. To measure the moisture content experimentally, the initial weight of sample with the crucible is first measured as denoted by W_0. Thereafter, the crucible containing the sample is kept in a stove at fixed temperatures between 120 – 150 °C for 3-4 hours (Mazumder et al., 2014). The resulting dry weight of the sample and crucible toghether is then measured as denoted by W. W_{S0} signifies initial sample weight (Garcìa-Cubero et al., 2009; 2013). In equation form, moisture content (MC) as expressed in the Eq.1:

$$MC\ (\%) = \frac{W_0 - W}{W_{S0}} * 100 \qquad (1)$$

Water is required for the growth and development of living trees and constitutes a major portion of green wood anatomy. In living trees, moisture content depends on the species and the type of-wood, and may range from approximately 25% to more than 250% (two and a half times the weight of the dry wood material). In most species, the moisture content of sapwood is higher than that of heartwood. Water exists in wood either as bound water (in the cell wall) or free water (in the cell cavity). As bound water, it is bonded (via secondary or hydrogen bonds) within the wood cell walls. As free water, it is simply present in the cell cavities. When wood dries, most free water separates at a faster rate than bound water because of accessibility and the absence of secondary bonding. The moisture content at which the cell walls are still saturated but virtually no water exists in the cell cavities is called the fiber saturation point. The fiber saturation point usually varies between 21 and 28% (Winandy, 1994).

Wood is a hydroscopic material that absorbs moisture in a humid environment and loses moisture in a dry environment. As a result, the moisture content of wood is a function of atmospheric conditions and depends on the relative humidity and temperature of the surrounding air. Under constant conditions of temperature and humidity, wood reaches an equilibrium moisture content (EMC) at which it is neither gaining nor losing moisture. The EMC represents a balance point where the wood is in equilibrium with its environment. In structural applications, the moisture content of wood is almost always undergoing some changes as temperature and humidity conditions vary. These changes are usually gradual and short-term fluctuations that influence only the surface of the wood. The time required for wood to reach the EMC depends on the size and permeability of the member, the temperature, and the difference between the moisture content of the member and the EMC potential of that environment. Changes in moisture content cannot be entirely stopped but can be retarded by coatings or treatments applied to the wood surface.

Elastic proprieties

Twelve constants (nine are independent) are needed to describe the elastic behavior of wood: three moduli of elasticity *E*, three moduli of rigidity *G*, and six Poisson's ratios μ (Green et al., 1999). The moduli of elasticity and Poisson's ratios are related by expressions of the form of the Eq.2

$$\frac{\mu_{ij}}{E_i} = \frac{\mu_{ji}}{E_j} \quad i \neq j \;\; i,j = L,R,T \tag{2}$$

Moduli of elasticity: elasticity implies that deformations produced by low stress are completely recoverable after loads are removed. When loaded to higher stress levels, plastic deformation or failure occurs. The three moduli of elasticity, which are denoted by E_L, E_R, and E_T, respectively, are the elastic moduli along the longitudinal, radial, and tangential axes of wood (Winandy, 1994; Green et al., 1999).

Poisson's ratios : when a member is loaded axially, the deformation perpendicular to the direction of the load is proportional to the deformation parallel to the direction of the load. The ratio of the transverse to axial strain is called Poisson's ratio. The Poisson's ratios are denoted by μ_{LR}, μ_{RL}, μ_{LT}, μ_{TL}, μ_{RT}, and μ_{TR}. The first letter of the subscript refers to direction of applied stress and the second letter to direction of lateral deformation. For example, μ_{LR} is the Poisson's ratio for deformation along the radial axis caused by stress along the longitudinal axis.

Modulus of rigidity : the modulus of rigidity, also called shear modulus, indicates the resistance to deflection of a member caused by shear stresses. The three moduli of rigidity denoted by G_{LR}, G_{LT}, and G_{RT} are the elastic constants in the *LR*, *LT*, and *RT* planes, respectively. For example, G_{LR} is the modulus of rigidity based on shear strain in the *LR* plane and shear stresses in the *LT* and *RT* planes (Green et al., 1999).

General relations between stress and strain for a homogeneous orthotropic material are related to anisotropic elasticity.

Anisotropy of the wood

The anisotropy of the wood is due to the bond between the microfibrils.

The bond that allows the conjunction of the individual glucose units is stable (60-80 cal / mol) and not easily divisible. Furthermore, on the cellulose chain are numerous hydroxyl groups (R-OH) which can, with other similar groups, form hydrogen bonds. Compared to previous, these bonds are characterized by an energy much lower (3-5 cal / mol). However the large number of hydrogen bonds allows the cellulose chains to bind to each other.

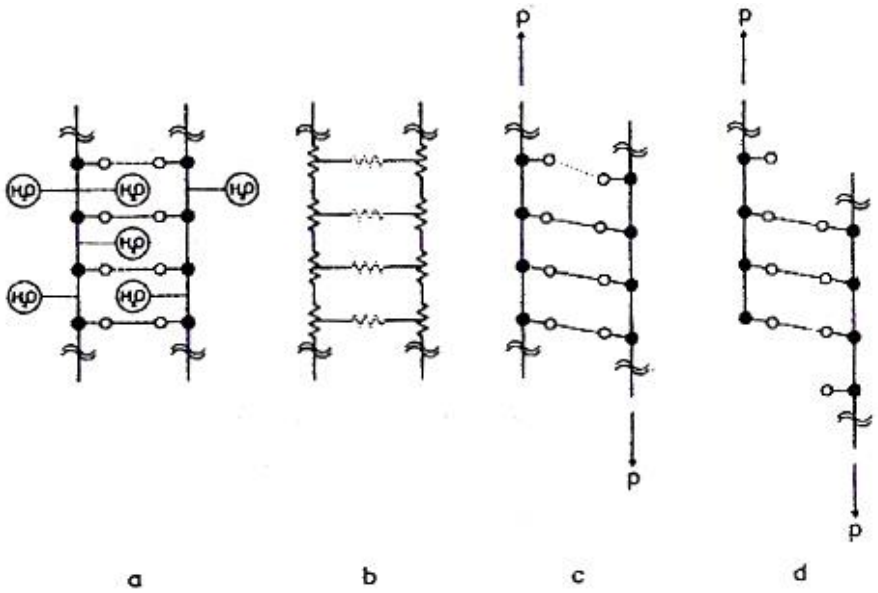

Figure 1.8 *Relations between the ultrastructural organization and deformability of wood: a) drawing of polisaccariche chains with water molecules linked b) schematic of the bonds as elastic connections ("springs" stiffer in longitudinal bonds of cellulose chains, weaker in hydrogen bonds) c) the solicitation P produces a deformation of the hydrogen bonds d) the solicitation P produces breakage and rearrangement of the bonds and consequent permanent deformation*

Due to the reduced hydrogen bond energy, the behavior of the microfibrils is anisotropic, with modest resistance to transverse stresses (Fig. 1.8d). Therefore the presence of the two different types of bond explains the different mechanical behavior with respect to the transverse or longitudinal stresses.

Not all of the hydroxyl groups (R-OH) are engaged in the structure of microfibril. In the amorphous zone some of these remain free and become the coupling point for the water molecules, which bind via hydrogen bonds. The number of groups (-OH) which remain available within the microfibrils is very high but finite, whereby the amount of water that the wood can keep directly linked to its structure is limited (*saturation water*).

The perfectly dry wood is virtually non-existent in nature. Moisture affects significantly on all the technological characteristics of the wood (dimensional changes, mechanical strength, elasticity, weight, etc.) and seriously affects the conservation of wooden artefacts. Tree, standing water is present both within the cell lumens (free water or imbibition) is wedged inside of the cell walls (saturation water). It defines the saturation point of the cell walls the moisture value of the wood at which all the imbibition water has been eliminated, while the whole of the saturation water is still bound to the cell walls. The value of the saturation point depends on various factors and can indicatively vary between 22% and 40%, but for most practical purposes it is sufficient to consider the conventionally fixed at 30% saturation point. The importance of the saturation point consists in

the fact that it marks a sort of threshold below which the wood begins to present considerable variations of its physical-mechanical properties with changes in humidity. When its moisture drops below about 30%, the wood is reduced in volume, is deformed, it can crack, it is more rigid and resistant to stress, while there was no significant differences (except of course the weight) when the same timber passes p. eg. from 200% to 40% moisture.

Hygroscopic equilibrium

Cell-wall substance is hygroscopic - that is, wood has the capacibility of exchanging bound water in the cell walls by adsorption or desorption directly with the atmosphere.

A speed difference between these two phenomena (always concurrent) causes the wood moisture variations (adsorption, if this increases; desorption, if this decreases), while identical speeds correspond to a situation of hygroscopic balance between the wood and the surrounding air. As reported in the work of Giordano (1981), the wood tends to equilibrate with the relative humidity of the surrounding air. In a first approximation, the equilibrium values are similar for all wood species, and depend only on temperature and humidity conditions of the environment, as shown in Tab. 1.1.

Relative Air Umidity	Temperature (°C)									
	0°	10°	20°	30°	40°	50°	60°	70°	80°	90°
5 %	1 %	1 %	1 %	1 %	1 %	1 %	1 %	1 %	1 %	1 %
10 %	3 %	3 %	3 %	2 %	2 %	2 %	2 %	2 %	1 %	1 %
15 %	4 %	4 %	4 %	3 %	3 %	3 %	3 %	2 %	2 %	2 %
20 %	5 %	5 %	5 %	4 %	4 %	4 %	3 %	3 %	3 %	2 %
25 %	6 %	5 %	5 %	5 %	5 %	5 %	4 %	4 %	3 %	3 %
30 %	6 %	6 %	6 %	6 %	6 %	5 %	5 %	4 %	4 %	3 %
35 %	7 %	7 %	7 %	7 %	6 %	6 %	5 %	5 %	4 %	4 %
40 %	8 %	8 %	8 %	7 %	7 %	7 %	6 %	6 %	5 %	4 %
45 %	9 %	9 %	9 %	8 %	8 %	7 %	7 %	6 %	6 %	5 %
50 %	10 %	10 %	9 %	9 %	9 %	8 %	7 %	7 %	6 %	6 %
55 %	11 %	10 %	10 %	10 %	9 %	9 %	8 %	7 %	7 %	6 %
60 %	12 %	11 %	11 %	11 %	10 %	10 %	9 %	8 %	7 %	7 %
65 %	13 %	12 %	12 %	12 %	11 %	10 %	10 %	9 %	8 %	8 %
70 %	14 %	14 %	13 %	13 %	12 %	11%	11 %	10 %	9 %	8 %
75 %	15 %	15 %	15 %	14 %	13 %	13 %	12 %	11 %	10 %	9 %
80 %	17 %	17 %	16 %	16 %	15 %	14 %	14 %	13 %	12 %	11 %
85 %	19 %	19 %	18 %	18 %	17 %	16 %	15 %	14 %	13 %	12 %
90 %	22 %	22 %	21 %	20 %	19 %	18 %	17 %	16 %	15 %	14 %
95 %	27 %	26 %	25 %	24 %	23 %	22 %	21 %	20 %	19 %	18 %
100 %	33 %	32 %	31 %	30 %	29 %	28 %	27 %	26 %	25 %	24 %

Table 1.1. *Values of equilibrium moisture of the wood: relative humidity in function of the air temperature (adapted from Giordano,1981). Approximately the reported relationships are referable to all wood species, with scraps of 2-3% humidity for the richest species of extractives.*

When wood is seasoned, the amount of bond water that is lost, as well as the amount that remains in the wood, is determined by the Releted Umidity (RH) of the atmosphere in which the drying is

completed. After initial drying, wood remains hygroscopic. It responds to changes in atmospherical humidity and loses bound water as RH decreases, or regains bound water as RH increases. The moisture condition established when the amount of bound water is in balance with the ambient RH is called the Equilibrium Moisture Content (EMC). The extremely important relationship between EMC and RH is shown in Figure 1.9.

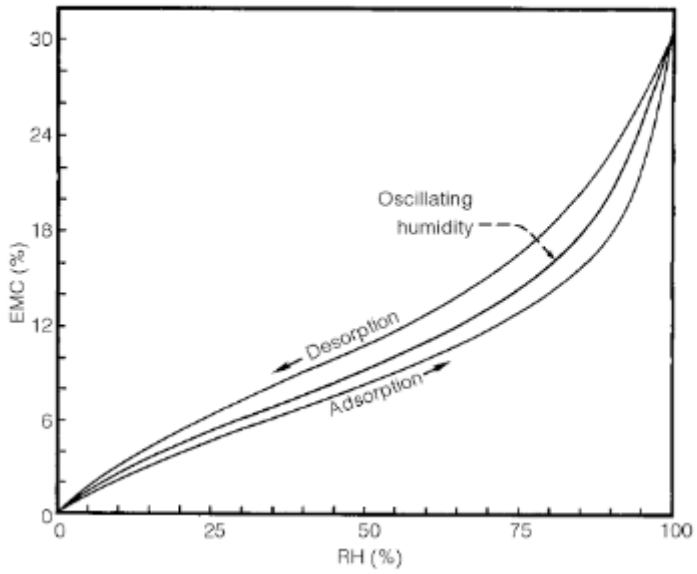

Figure 1.9 *Relationship between environmental RH and EMC for wood. The hysteresis effect is indicated by the different curves for desorption and adsorption in thin speciemens under carefully controlled conditions. in the natural environment, with its fluctating humidity, wood of lumber thickness attains average MCs as indicated by the oscillating humidity curve (adapted from Hoadley, 1998)*

The figure extrapolated by a work of Hoadley (1998) contains average data for white spuce, a typical species, shown an having an Fiber Saturation Point (FSP) of about 30% of the moisture content. The FSP varies somewhat among different species: for wood having a high extractive content, such as rosewood or mahogany, the FSP can be as low as 22-24%; for those low in extractives, such as beech or birch, the FSP might be as high as 32-34%. Temperature also has an effect on EMC. the curves shown are for 21°C, but at intermediate humidities the EMC would be about one percentage point lower for every 14-16 °C elevation in temperature. The EMC curves always converge at 0% RH and 0% EMC, so variation due to extractives and temperature will therefore be most pronunced toward the FSP end of the relationship.

under conditions in witch the RH is closely controlled, the curve for wood that is losing moisture (a desorption curve) is significantly higher than the curve for wood that is gaining moisture (an adsorption curve), as illustrated in Figure 1.9. this effect is called hysteresis. During the conditioning of wooden objects under precisely controlled laboratory conditions, the hysteresis

effect may be apparent. Under normal room or outdoor conditions of fluctating RH, an averaging effect results, usually referred to as the oscillating curve (Hoadley, 1998).

References

García-Cubero M., T., González-Benito, G., Indacoechea, I., Coca, M., Bolado, S., 2009. Effect of ozonolysis pretreatment on enzymatic digestibility of wheat and rye straw. *Bioresource Technology*, 100, 1608–1613.

García-Cubero, M.T., González-Benito, G., Indacoechea, I., Coca, M., Bolado, S., 2013. Biomass proximate analysis using thermogravimetry. *Bioresource Technology*, 139, 1-4.

Giordano, G., 1981. *Tecnologia del legno.* vol. I, UTET, Torino.

Green, D., W., Winandy, J., E., Kretschmann, D., E., 1999. Mechanical properties of wood. USDA (ed.) Wood handbook: wood as an engineering material. Madison, USDA Forest Service, Forest Products Laboratory. General technical report; pp. 4.1-4.45

Hendriks, A.T.W.M., Zeeman, G., 2009. Pretreatments to enhance the digestibility of lignocellulosic biomass. Bioresource Technology, 100, 10–18.

Hoadley, R.,B., 1998. Wood as a Physical Surface for Paint Application. In: , Dorge, V., Howlett, F.,C., (eds), Painted Wood: History and Conservation. Proceedings of a Symposium Organized by the Wooden Artifacts Group of the American Institute for Conservation of Historic and Artistic Works, *Williamsburg, Virginia, 11–14 November 1994*. Los Angeles: The Getty Conservation Institute, pp. 2–16.

Kumar, P., Barrett, D.M., Delwiche, M.J., Stroeve, P., 2009. Methods for Pretreatment of Lignocellulosic Biomass for Efficient Hydrolysis and Biofuel Production. Industrial and Engineering Chemistry Research, 48 (8), 3713–3729.

Mazumder, A., Maity, S., Sen, D., Gayen, K., 2015. Process Development For Hydrolysate Optimization From Lignocellulosic Biomass Towards Biofuel Production In: Basile, A., Dalena, F. (eds.), Alcohols and bioalcohols Characteristics, Production and Uses, Nova Publisher Chapter 3, 41-75

Pettersen, R.C., 1984. The Chemical Composition of Wood. Advances in chemistry, 207, 57–126.

Ritter, S.K., 2008. Lignocellulose: A Complex Biomaterial. Plant Biochemistry, 86 (49):15.

Sanderson K, 2011. Lignocellulose: A chewy problem. Nature, 474, S12–S14.

Sloneker , J.H., 1971. Determination of Cellulose and Apparent Hemicellulose In Plant Tissue by Gas-Liquid Chromatography. Analytical Biochemistry, 43, 539-546.

Sun, Y., Cheng, J., 2002. Hydrolysis of lignocellulosic materials for ethanol production: a review. Bioresource Technology, 83, 1–11.

Taherzadeh, M.J., Karimi, K., 2007. Acid based hydrolysis for ethanol from lignocellulosic materials: A review. BioResources, 2 (3), 472-499.

Ververis, C., Georghiou, K., Christodoulakis, N., Santas, P., Santas, R., 2004. Fiber dimensions, lignin and cellulose content of various plant materials and their suitability for paper production. Industrial Crops and Products, 19, 245–254.

Winandy, J.,E., 1994. Wood Properties, In: Arntzen, C., J.(ed.), Encyclopedia of Agricultural Science. Orlando, FL: Academic Press, 549-561. Vol. 4. October 1994.

Chapter 2

Insect-Infested Wood Remediation by microwave heating and its effects on wood dehydration: a case study of *Hylotrupes bajulus* larva

Wood artefacts are subject to damage by biologic infestations due to bacteria, insects, and fungal species. One of the worst feared attack is due to the xylophagous insects which larvae feed on wood by boring galleries, at the expense of building timbers and worked woods. These beetles are responsible for a day by day destruction of the world wooden cultural heritage, and their elimination has been always a big problem for conservation of wood. The need to avoid the use of chemical methods in conservation for pest control, has led to the development of various non-chemical, non-toxic treatments. Among these, heating with microwaves (MW) seems to be one of the most promising, since it has already been shown its high efficacy in destroying pest. MW treatment in conservation is based on the larger heating effect caused by exposure to these radiations on larvae than in wood, due to their different dielectric permittivity in the GHz range. However, the side effects that may occur due to MW-heating of wood, such as dehydration, have not been discussed so far. Here we study the possible application of microwaves heating as a remediation method for wood samples infested by the larvae of the insect *Hylotrupes bajulus*. Here we show that it is possible to set-up exposure conditions able to achieve the 100% of the larva worms death and that are sufficiently mild to not induce significant dehydration of the exposed wood from which shrinkage effects may derive.

Indeed, under these conditions, MW-induced wood dehydration on cubic and parallelepiped chest

Chidichimo, G., Dalena, F., Rizza, A., Beneduci, A., 2017. Wood disinfestations from larval *Hilotrupes baiolus* by microwave radiation: effects on wood dehydration. Studies in Conservation, 1-7. ARTICLE IN PRESS

nut samples, can be kept under control and to percentages as low as 0.4% (w/w).

2.1 Introduction

Any wood artefact is an ideal incubator for xylophagous insects as their larvae feed on wood and develop, up to the adult stage, at the expense of building timbers and worked woods. Depending on the species of insect and on factors such as nutrient quality of the infested wood, temperature and hygrometry, larval development may last up to 10 years. During this stage, larvae bore galleries in the wood, undermining the structural integrity of architectural masterpieces, thus eroding our cultural heritage. An example of this erosion is shown in Figure 2.1. The figure shown SEM images (Scanning Electron Microscope) related to wood samples infested by wood pests. From the figure it can be noted the apparent embrittlement of wood.

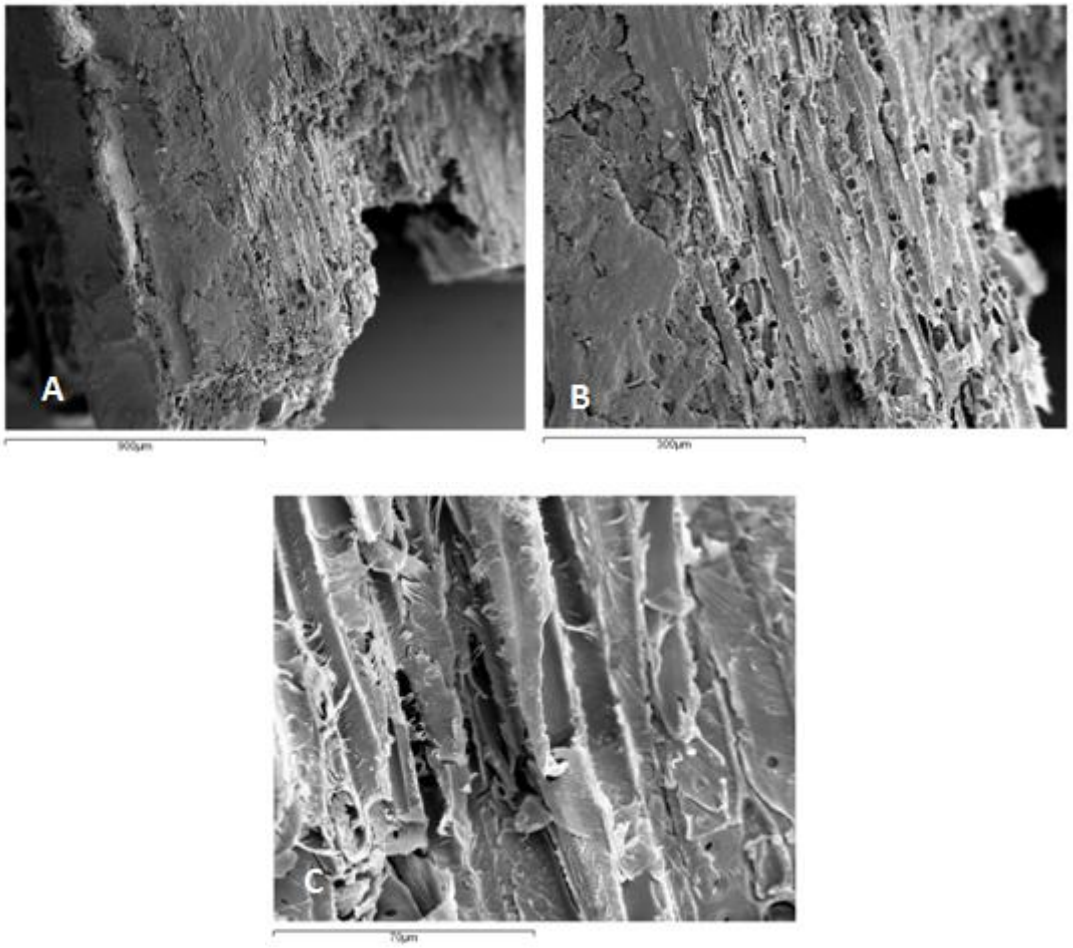

Figure 2.1. *SEM images related to wood samples infested by wood pests at three magnifications scale: 900 µm (A), 300 µm (B) and 70 µm (C)*

Common conservation treatments are based on the exposure of artefacts to chemicals (Lewis 1997; Lewis & Haverty, 1996) such as aerosol pyrethrum, aerosol and liquid pyrethroids (cyluthrin, permethrin, bifenthrin), liquid imidacloprid, liquid nitrogen, liquid and dust formulations of disodium octaborate tetrahydrate (Plaza *et al.*, 2007). Chemical wood preservatives are directly applied to the wood by spraying or brushing its surfaces or by dipping the target wood and should be therefore carefully handled by trained and informed operators due to the potential risks associated to accidental exposure to such toxic substances. These methodologies have the further inconvenient to be not effective in destroying the eggs of the insects. Thus, the public is showing increased interest in non-chemical, non-toxic methods for pest control. For instance, electrocution is based on high voltage- low current devices. However, it has an effectiveness as low as 44% (Lewis and Haverty, 1996). Other methods prescribe exposure of artefacts to controlled atmosphere such nitrogen and argon fumigation CO_2 fumigation (Unger et al., 2011; Selwitz and Maekawa, 1998) or exposure to vacuum (Chidichimo et al., 2015), where low oxygen concentrations are achieved. Alternative, most promising methods are those that expose the objects to high temperatures These include conventional heating over lethal levels (above 53 ºC) for at least 33 minutes (Lewis & Haverty, 1996). solarisation in specifically designed "solar tents" which makes use of the solar energy radiation to heat the target materials covered by a transparent plastic film or glass (Strang 1995, Strange et al., 1992; Brokerhof, 1999; 2001; 2004). However, any heat treatment may induce side effects on low-melting point materials of museum objects, that are sensitive to the high temperatures achieved during heating. Moreover, wood dehydration could be a major drawback for the integrity of wood artefacts. One heating method that could potentially overcome such issues is exposure to microwaves(MW) that are electromagnetic radiation with frequency in the range 300 MHz-300 GHz., MW heating relies on the differential temperature increase of pests and the infested materials, due to their different dielectric properties at microwave frequencies. Indeed, the microwave power absorbed by the exposed object (P_D) is strictly dependent on its dielectric properties and is given by the following expression (Beneduci et al. 2012, 2014; Das, A. , 2007.):

$$\begin{aligned} P_D &= \sigma\left|E_i\right|^2 = \omega\varepsilon_0\varepsilon''\left|E_i\right|^2 \quad (W/m^3) \\ \sigma &= \omega\varepsilon_0\varepsilon''(S/m) \end{aligned} \tag{3}$$

where, σ is the medium conductivity that is proportional to the angular frequency ω of the electromagnetic field and to the loss factor $\varepsilon_0\varepsilon''$of the exposed material, and E_i is the internal electric field.

It follows that the temperature rise of the exposed object is proportional to the power absorbed and, in the first few seconds of exposure over which heat diffusion and convection do not occur, the time rate of initial temperature rises dT/dt , is given by (Eq. (4)):

$$\frac{dT}{dt} = \frac{P_D}{cV\rho} \quad (K/s) \qquad (4)$$

where dT is the temperature increment, dt is the duration (sec) over which T is measured, c is the specific heat (J/kg-K), V (m^3) the volume and ρ (kg/m^3) the density of the material.

From equations 3 and 4 it is clear that the temperature rise in the exposed object is strictly dependent on the incident power and on its material properties, i.e., dielectric, density, volume, specific heat. At a given incident power, the T increase is proportional to the dielectric loss factor (ε'') and inversely proportional to the other material parameters.

Notably, typical dielectric permittivity values of wood at room temperature and at 2 GHz are ε'~ 2.5, ε''~ 0.2 while typical values for some insect larvae are ε'~ 45, ε''~ 15 (Wang et al., 2010). That is, the dispersive part of the permittivity, the so called loss factor ε'', responsible for the adsorption of microwave energy in the material, is about two orders of magnitude higher in the insect pest than in wood, bringing the attention to the fully potentialities of MW heating for pest control in conservation.

At microwave frequencies, the dielectric properties of a material are heavily affected by its water content. Since water is a strong absorber of MW energy (Beneduci, 2008, Beneduci 2012), the higher the water content, as in the case of woodworm compared to wood, the higher the values of dielectric loss factor of the material, responsible for microwave absorption. Therefore, MW exposure should, in principle, induce higher temperatures rise in the larva's bodies than in wood, in order to kill the exposed larva while preserving undesired wood dehydration, which ultimately could affect the structural integrity of the wood artefact. The optimal exposure conditions, i.e., MW power, exposure duration, exposure temperature, etc., should be kept under control in order to minimize any MW-induced wood dehydration effect and to maximize pest remediation. Early works on the use of MW for pest control in wood have attempted to determine the lethal temperature of a particular woodworm (Hylotrupes bajulus L.) (Andreuccetti *et al.,* 1995a). Results have demonstrated that this is a function of the larva weight but is confined to a narrow range between 52-53 °C (Andreuccetti *et al.,* 1995b; Bini *et al.,* 1997a; Bini *et al.,* 1997b; Vivancos-Ramon *et al.,* 2006). More recently, dielectric heating, which includes both radio and microwave frequency heating, has been investigated for insect disinfestation (Jiao *et al.,* 2011; Nelson & Trabelsi, 2012; Jian *et al.,* 2015). Results have pointed out that the uneven temperature distribution

of the exposed materials depends on many factors such as microwave oven structure/dimension, magnetron configuration and power, depth, and dielectric properties of the treated materials (Kelen *et al.,* 2006). The dielectric properties of biological materials also depend on the frequencies used and on the composition, moisture content and temperature of the treated materials. Several possible solutions have been suggested to avoid the undesired temperature non-uniformity and moisture content, e.g., intensifying the mixer motion, reducing microwave power, and adding hot air (Jian *et al.,* 2015; Kelen *et al.,* 2006; Jiao *et al.,* 2012). However, an increase of the mixer motion can decrease the non-uniformity only to a certain level (Pan *et al.,* 2012) and most domestic microwave ovens are usually equipped with a rotating plate. Any decrease in microwave power will increase the treatment time. Moreover, even though, adding hot air can improve heating uniformity (Jian, *et al.,* 2015; Kelen, *et al.,* 2006; Jiao, *et al.,* 2012; Pan, *et al.,* 2012; Wang, *et al.,* 2010), it will also increase the complexity and cost of the microwave or radio frequency treatment. It has been suggested that an intermittent microwave treatment might decrease the non-uniformity and could be more effective in killing insects than continuous irradiation (Shayesteh, & Barthakur *et al.,* 1996).
We are interested to develop wood disinfestations in large microwave ovens to preserve the workers with respect to accidental MW exposure. For this reason, here we present an experimentation of woodworm treatments in a MW oven: the aim is to find the minimum MW energy density and exposure treatment time to disinfect walnut wood (*Liquidambar styraciflua*) from the house longhorn beetle *Hylotrupes bajulus* larvas, one of the most effective destroyer of wood, and to study the amount of wood dehydration under these effective exposure conditions of artefacts. First, data on the minimum lethal exposure will be presented and then, the effect on wood dehydration will be discussed.

2.2 Experimental

MW exposure was carried out by a MOULINEX MW oven with internal dimensions 330 cm x 310 cm x 210 cm, at 2450 MHz and an output power (P) ranging from 100 up to 900 W. The average incident power density (P_D) inside the oven was estimated by dividing P with the inside volume (V) of the oven:

$$P_D = \frac{P}{V} \quad (W/m^3) \tag{5}$$

MW exposure of larvae

In order to perform a significant number of experiments, Hylotrupes bajulus larvae were breed in a chestnut wood incubator already infested by the worms. Chestnut wood trunks (10 cm in diameter by 30 cm in length as an average) were kept for 9 months at 20°C and a relative humidity of 70% in aerated conditions. These environmental parameters allowed an optimal growth of the number of larvas to feed our experiments. Figure 2.2 A gives an idea of the breeding substrate.

The box in walnut wood illustrated in the next Figure 2.2 B was used to simulate the habitat of worms in the wood, during MW experiments. This container allowed to monitor the effectiveness of the irradiation by simply visual inspection of the larvas.

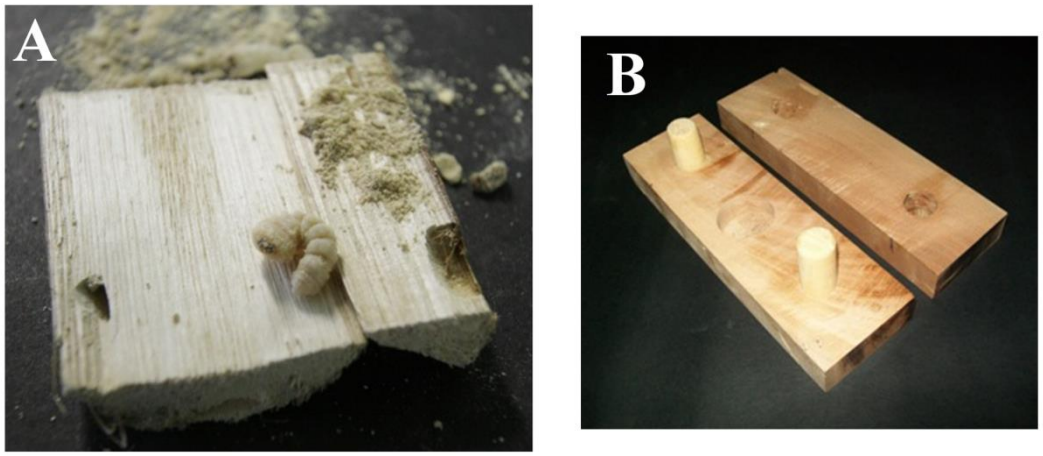

Figure 2.2. *A) Breeding substrate for Hylotrupes bajulus larvas; B) Experimental setup used to investigate the effect of MW exposure on worm healt condition (dimensions of the closed container= 20cmx6cmx4cm; diametr of the internal lodging= 3cm).*

MW exposure experiments were performed by placing the wood box containing worms, in the center of the MW oven. Exposure was performed at two different power densities, namely 4.65×10^{-3} watt/m^3 and 8.33×10^{-3} watt/m^3, and for times starting from 30 seconds and gradually increased by steps of 30 s up to 240 s. After the exposure, the wood box was extracted from the oven and the temperature in the wood cavity measured by a *Fluke 52 k/J thermometer* having a flat detector thermocouple. Immediately after exposure, worms were preliminary analysed by visual inspection of their apparent conditions (color, shape, activity). The state of health of the exposed worms was then evaluated by monitoring their mobility for at least two hours (by a video recording device). Worms that did not show any mobility during this time of observation were considered dead. Moreover, the worm death could also be confirmed by its evident withering and colour change. For each exposure time, 10 worms directly extracted from the breeding site, were monitored. The

results reported below come from 6 replicates for each exposure experiments. In this way, for each MW exposure condition, data relative to 60 worms were used for statistical analysis.

Effect of MW exposure on wood dehydration

In order to investigate the dehydration of wood induced by MW at the same power densities used in the worms exposure experiments, walnut wood samples with various geometries were analysed, since it is expected that the field distribution inside the wood samples is a function of their shape. More precisely, the water lost by cubic wood samples of 1.5 cm, 2.0 cm, 3.5 cm, 4.0 cm side dimensions, and by parallelepiped samples having dimensions of 2.0 cm x 4.0 cm x16 cm, was measured as a function of the exposure time. Moreover, since the field distribution inside the wood samples with parallelepiped geometry, that is the dielectric heating effect, it is expected to depend also on the orientation of the parallelepiped with respect to the microwave source, experiments were performed for different orientations of the samples.
The amount of water lost was obtained by measuring the weight difference of wood sample before (w_i) and after exposure (w_f) intervals of nx60 sec with n= 1, 2, 3,…. The percentage of lost water was calculated as:

$$\text{Water loss \%} = \frac{w_i - w_f}{w_i} \times 100 \qquad (6)$$

For each of the experiment corresponding to a given exposure time and power a fresh sample was used. Wood samples were conditioned for 10 months at a relative humidity of 45% and at a temperature of 20 °C. In these conditions, all samples contained the 12.03±0.01 % of water. This data was obtained according to UNI ISO 3130 standards (Nelson & Trabelsi, 2012).

2.3 Results and discussion

MW exposure effect on worm viability

The effectiveness of the microwave exposure treatment at the two power densities used (8.37×10^{-3} watt/m^3 and 4.65×10^{-3} watt/m^3), in terms of worm death percentage, is reported in Figure 2.3. Data on the percentage of larvas death under MW exposure are plotted in Figure 2.3A as a function of

the power density and of the exposure time. It can be seen that, at both the power densities used, there is a time threshold above which MW exposure induces the death of the larvas.

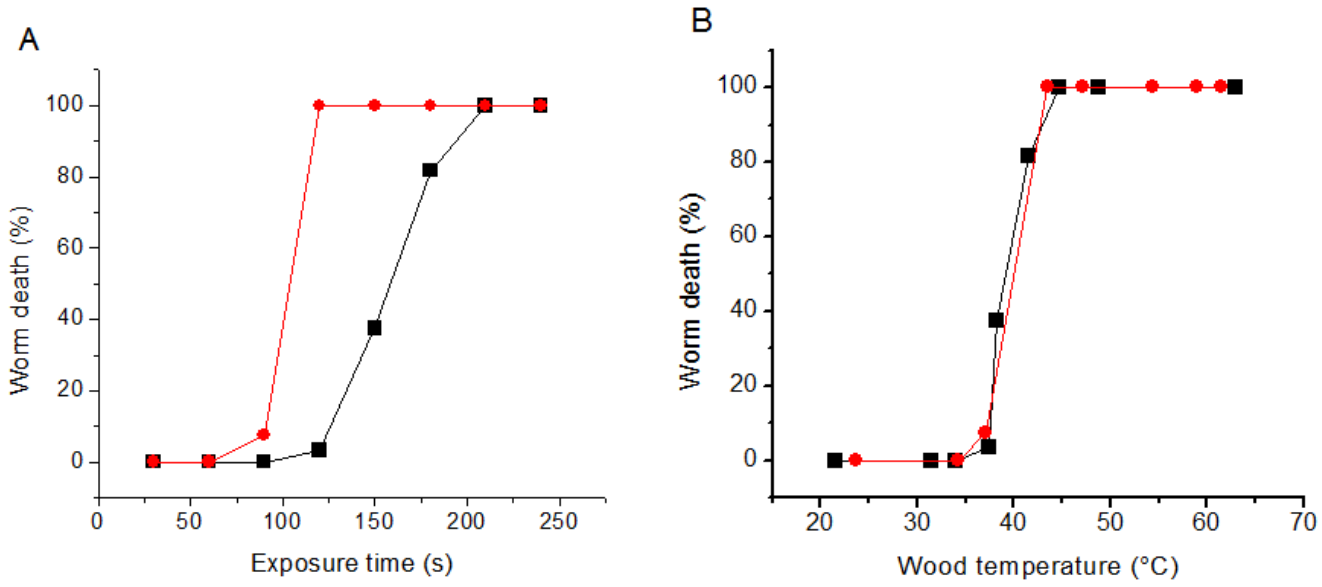

Figure 2.3. *A) Trend of worms percentage death as a function of the exposure time at a power density of 4.65 ×10^{-3} watt/m^3 (■) and 8.37×10^{-3} watt/m^3 (●); B) worm death percentage as a function of the temperatures reached by the experimental wood box used in the experiments (see fig 2.2) at a power density of 4.65 ×10^{-3} watt/m^3 (■) and 8.37×10^{-3} watt/m^3 (●).*

Such a threshold depends on the MW power density, being lower for higher power density (about 70 s and 120 s respectively at 8.37 ×10^{-3} watt/m^3 and 4.65 ×10^{-3} watt/m^3). Above the threshold, the percentage of larvas death exhibits a stepwise increase with a MW power density dependent slope, leading to a 100% larvas death after about 120 s and 210 s respectively at 8.37×10^{-3} watt/m^3 and 4.65 ×10^{-3} watt/m^3.

Figure 2.3B shows the % of larvas death as a function of the temperature rise measured in the wood box after exposure. These plots show that there is a proportionality relationship between the temperature of the wood container and the percentage of larvae death. It is worth noting that this correlation is the same for both the power densities used. Even though, we could not measure the temperature rise induced on the larvae by MW exposure, we should expect that this is proportional to the temperatures rise of the wood container, such that a proportionality relationship holds true between the % worms death and the MW induced temperatures rise of the larva body. At a first glance, the highest power density appears to be more convenient since less time is used to kill the totality of worms and therefore, less exposure time to wood. We will see that this conclusion must be changed when taking into consideration the data on water dehydration of wood, that will be discussed below.

Water lost in walnut wood samples under MW exposure

Figure 2.4 reports the percentage of water lost by cubic samples of walnut wood, for different sample sizes, at a power density of 4.65×10^{-3} watt/m^3 and 8.37×10^{-3} watt/m^3, as a function of the exposure times.

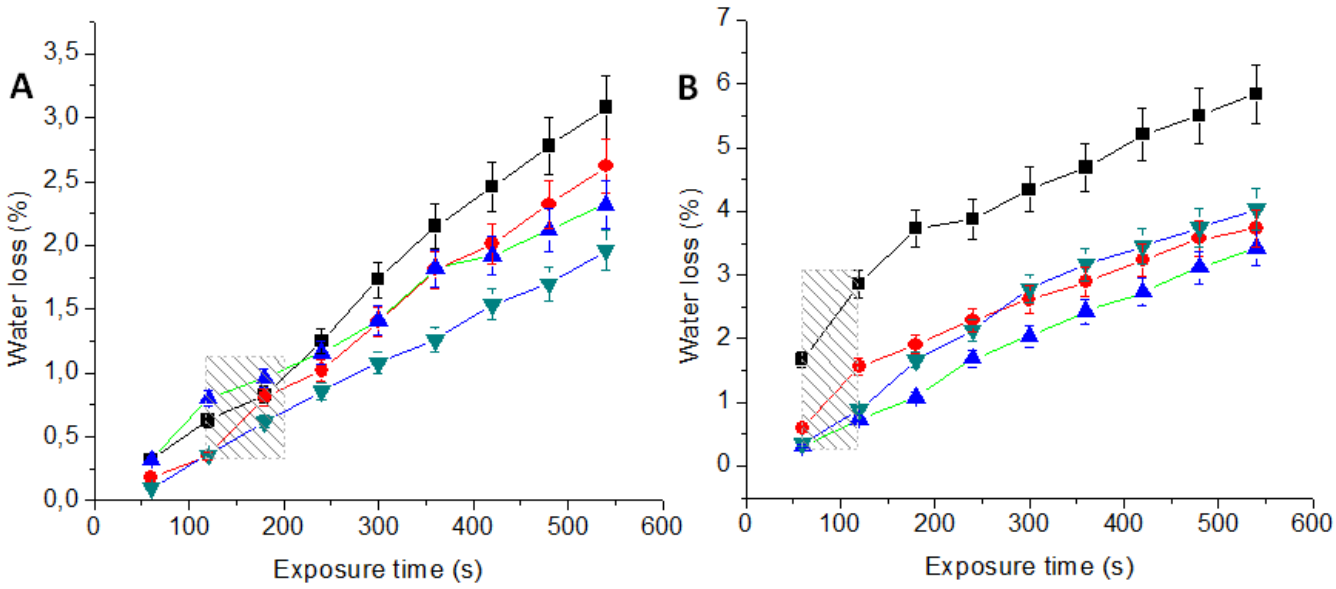

Figure 2.4. *Percentage of water lost from cubic wood samples having side of 1.5cm (■), 2.0 cm (●), 3.5cm (▲), 4.0 cm (▼) as a function of the MW exposure time, at a power density of 4.65 ×10^{-3} watt/m^3 (A) and 8.37 ×10^{-3} watt/m^3 (B). The dashed areas indicates the approximate relationship between the exposure time dependent worm death and the exposure time dependent wood dehydration.*

Figure 2.4 shows that the loss of water from the wood, monotonically increases with the exposure time. As expected, for the same exposure time, the loss of water is larger at the highest power density used, reaching values as high as 5.5 % after 550 s. Moreover, the water contained in the exposed samples is more quickly lost in the sample with smaller dimensions. This is due to the fact that the water molecules need to reach the surface of the wood to evaporate. The less is the path to cover to reach the surface the greater the speed of evaporation.

The dashed rectangular areas sketched in the plots shows the approximate relationship between the exposure time dependent worm death and the exposure time dependent wood dehydration. The time dimension of these rectangles includes the exposure time interval in which the MW exposure induces the worm death (see Figure 2.3A). It can be seen that, at an exposure time of about 200 s, corresponding to 100% of worms death at a power density of 4.65×10^{-3} watt/m^3 (Figure 2.3A), the loss of water from the wood samples is below 1%, and becomes as low as 0.4% in the case of the

ticker sample (4 cm cubic side). However, when the exposure power density is raised up to 8.37 $\times 10^{-3}$ watt/m^3, the water loss goes from 0.8% to almost 3% when going from the 4 cm side cubic sample to the 1.5 cm side one. On the basis of this result, it should be concluded that microwaves exposure at lower power densities should be preferred for conservation treatments in order to avoid a higher water loss of the exposed artefacts which may cause its shrinkage. Moreover, these milder heating conditions should also mitigate any potential adverse effect associated to the presence of resins (e.g. in pine), varnishes, and waxes that are low-melting materials that could experience a softening or a movement if the temperature rise achieved under MW exposure is above their transition temperatures.

Investigation of the dehydration anisotropy

The water loss in parallelepiped samples is shown in Figure 2.4 for three different power densities and for two different sample orientations: vertical, when the normal to the lowest surface is perpendicular to the direction of radiation propagation, and horizontal when the normal to the lowest surface is parallel to the direction of radiation propagation, with the widest face on the MW rotating plate. It can be seen that no anisotropic effects are induced at the power densities used in the larvas exposure experiments described above, i.e., at 4.65×10^{-3} watt/m^3 and 8.37×10^{-3} watt/m^3 . In contrast, at the highest power density used, the water loss becomes strongly dependent on the wood surface orientation. This suggest that, in real applications on wood artefacts, wood surfaces with different orientations would experience different water loss. This effect is caused by the different internal electric field distribution built-in during exposure inside the same sample in the two orientations, that is due the anisotropic dielectric properties of wood (Olmi et al. 2000). This effect should be avoided since it would introduce uncontrolled tensions on the artefacts due the differential shirking of surfaces undergoing to different water lost process. This effect could be controlled by choosing suitable exposure conditions in terms of either power density or artefacts orientation inside the oven. The data reported above show that efficient exposure power conditions can be applied where differential water loss is negligible and effective larvas death is achieved.

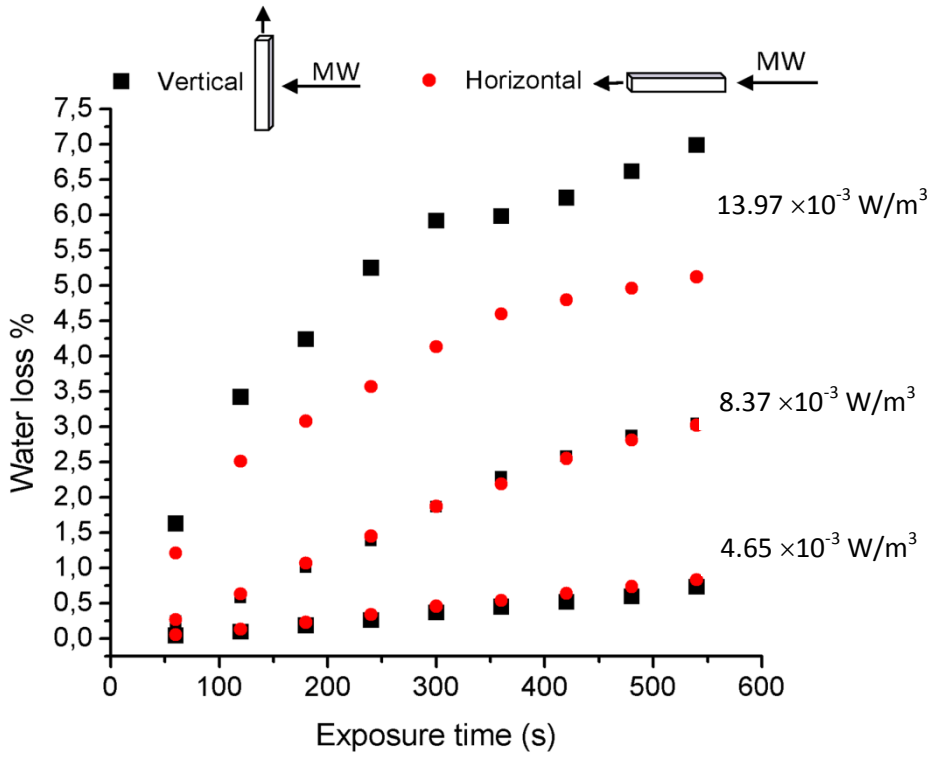

Figure 2.5. *Water lost by parallelepiped walnut wood samples 2.0 cm x 4.0 cm x16 cm in size for three different power densities (4.65 ×10^{-3} watt/m^3; 8.37×10^{-3} watt/m^3 and 13.96×10^{-3} Watt/m^3) and two different sample orientations with respect to wave propagation vector●horizontal orientation, ■ perpendicular orientation: see text and insets in the figure).*

SEM EDX analysis of the chemical stability of the wood in function of the microwave irradiation

This section shows the results of a survey conducted by SEM / EDX (*Scanning Electron Microscopy/Energy Dispersive: X-Ray Analysis*) spectroscopy to check if the weight loss observed following irradiation microwave are only attributable to the loss of reversible water timber and not to other degradation chemical. This semi-quantitative spectroscopic analysis allows to determine the relationship between the amount of oxygen and carbon present in the sample. The only loss of water should correspond to a rise of the Carbon/Oxygen ratio, since the loss of water is directly proportional to the presence of oxygen in the sample, but not to the amount of carbon. On the contrary, if the effect of the local heating would lead to a crushing of the wood molecules it would also have a greater loss of carbon. In other words, if the degradation of the wood is reversible, the irradiation must only correspond to a molecular water loss of the wood (directly proportional to the amount of O) with a relative decrease of the O / C ratio. On the contrary, if the degradation of the wood is irreversible, the irradiation also corresponds to the loss of C in the form of CO and CO_2,

being the wood composed of hemicellulose, lignin and cellulose (as discussed in Chapter 1). Then, the loss of C corresponds to a relative increase in the O / C ratio.

The analysis was performed on three of walnut wood samples, having an area of 1 cm^2 and a thickness of 3 mm. These samples are irradiated with microwaves for a time of 2 min., at a three different power densities (4.65 $\times 10^{-3}$ watt/m^3; 8.37$\times 10^{-3}$ watt/m^3 and 13.96$\times 10^{-3}$ Watt/m^3). and a similar non-irradiated sample, used in the experiment as compared to the calculus of variations.

The samples were deposited on the appropriate stubs and stored in a desiccator for 24 hours. The SEM / EDS has operated under vacuum conditions (10^{-6} atm) and the power of the incident beam is equal to 650 pA.

In the Figure 2.6 are reported the SEM-EDX spectra of the four analyzed wood samples. In the figure it has been highlighted the areas of the spectrum relating to the peaks relative to the carbon and oxygen.

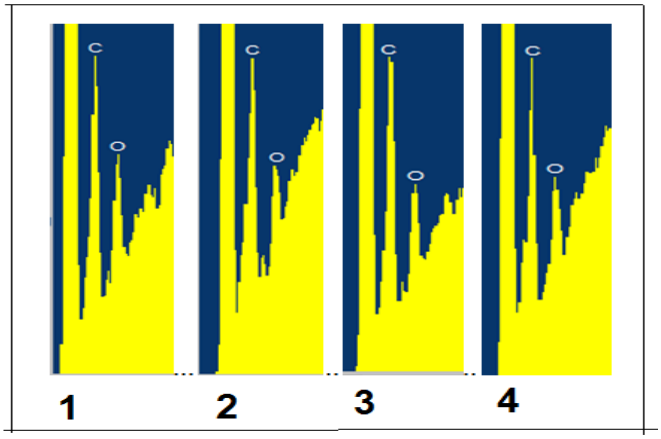

Figure 2.6. *SEM EDX spectra of four walnut wood samples. 1: non-irradiated sample; 2,3,4, the irradiated samples, at a three different power densities respectively 4.65 $\times 10^{-3}$ W/m^3; 8.37$\times 10^{-3}$ W/m^3 and 13.96$\times 10^{-3}$ W/m^3, for 2 minutes*

Below it is shown the table of results extrapolated by SEM / EDS spectrophotometer. The table shows the relationship between the percentage in weight of oxygen respect to the percentage in weight of the carbon obtained by the INCA software of the SEM-EDS

	non-irradiated sample	*4.65 ×10^{-3} W/m^3*	*8.37×10^{-3} W/m^3*	*13.96×10^{-3} W/m^3*
O/C%	***0,98***	***0,92***	***0,81***	***0,75***

Tab. 2.1 *Values expressed in weight percentage of the ratio Oxygen / Carbon extrapolated measured by SEM / EDS.*

As it can be seen in Tab.2.1, the report in a non-irradiated sample is almost equal to 1 (0.98).
In fact, the carbon present in terms of weight percentage is equal to 50.05, while the oxygen is equal to 49.05. For the irradiated sample at a power density equal to *4.65 ×10^{-3} W/m^3* tends to remain constant this ratio (0.92). Raising the power density, the sample loses a quantity of oxygen no longer negligible (0.81 for a power density equal to *8.37×10^{-3} W/m^3* and 0.75 for a power density equal to *13.96×10^{-3} W/m^3*). Therefore, the analysis carried out by SEM / EDS confirmed that the safe procedure to perform analysis by means of microwaves is equal to a density power of *4.65 ×10^{-3} W/m^3*. For higher powers, it would tend to increase the risk to the structural safety of the wood.

2.4 Conclusions

This part of research work reports an accurate investigation of the effectiveness of MW exposure to remediate pest-infested wood artefacts from larval *Hylotrupes bajulus*. Very effective exposure power densities and corresponding exposure times required to kill the 100% of larvas have been determined. It has been shown that the water loss from wood samples can be kept below 1% when appropriate experimental conditions are used. Moreover, it has also been shown that the percentage of water loss is not influenced by the relative orientations of wood surface with respect to the wavevector propagation, provided that the exposure power density is maintained below about 8×10^{-3} watt/m^3(Figure 2.5).

References

Andreuccetti, D., Bini, M., Ignesti, A., Gambetta, A. and Olmi, R., 1995a. Feasibility of Microwave Disinfestation of Wood. Proceedings of the 26th Annual Meeting IRG/WP. Helsingor, Denmark, June. doc. no. IRG/WP/95-40051.

Andreuccetti, D., Bini, M., Ignesti, A., Gambetta, A., Olmi, R., 1994. Microwave Destruction of Woodworms. Journal of Microwave Power and Electromagnetic Energy, 29, 153-160.

Andreuccetti, D., Bini, M., Ignesti, A., Olmi, R., Priori, S., Gambetta, A. and Vanni, R. 1995b. A microwave device for woodworm disinfestations. Proceedings of the International Conference on Microwave and High Frequency Heating, St John's College, Cambridge, UK.

Annapurna Das,Sisir K. Das, 2007 Microwave Engineering Tata McGrow-Hill Pu8blishing Company Limited, 2007, 439-444.

Arney, J. S., A. J. Jacobs, and R. Newman. 1979. Influence of oxygen on the fading of organic colourants. Journal of the American Institute for Conservation 18, 108-117. http://cool.conservation-us.org/jaic/articles/jaic18-02-004_indx.html

Beneduci, A. 2008. Which is the effective time scale of the fast Debye relaxation process in water? Journal of Molecular Liquids, 138, 55-60.

Beneduci, A. and Chidichimo, G., 2012. Open-ended waveguide measurement and numerical simulation of the reflectivity of Petri dish supported skin cell monolayers in the mm-wave range. Journal of Infrared, Millimeter, and Terahertz Waves, 33(5), 529-547.

Beneduci, A., Cosentino, K., Romeo, S., Massa, R., Chidichimo, G., 2014. Effect of millimetre waves on phosphatidylcholine membrane models: a non-thermal mechanism of interaction. Soft matter, 10(30), 5559-5567.

Beneduci, A., Filippelli, L., Cosentino, K, Calabrese M. L., Massa R. Chidichimo, G., 2012. Microwave induced shift of the main phase transition in phosphatidylcholine membranes. Bioelectrochemistry 84, 18–24.

Bini, M., Andreuccetti, D., Ignesti, A., Olmi, R., Priori, S. and Vanni, R. 1997. A Portable Microwave System for Woodworm Disinfestation of Artistic Painted Boards. Journal of Microwave Power and Electromagnetic Energy, 32, 180-187.

Bini, M., Andreuccetti, D., Ignesti, A., Olmi, R., Priori, S., Vanni, R., 1997a. Treatment Planning in Microwave Heating of Painted Wooden Boards. In: A. Breccia, R. De Leo, and A.C. Metaxas (eds)., Proceedings of the VI International Conference on Microwave and High Frequency Heating, Fermo (AP), Italy, 361-364.

Brokerhof, A.,W. , 1999. Low-oxygen treatment and solarisation of Probota iconostasis: alternative pest control methods in the field. In: J. Bridgeland (ed.) ICOM-CC 12th Triennial Meeting, Lyon 1999, ICOM-CC, Paris, 14-20.

Brokerhof, A.,W. , 2001. Solarisation; a cheap but effective method to disinfest museum objects. ICN/CSIRO Research Report, ICN, Amsterdam, 27 pp.

Burke, J. 1996. Anoxic Microenvironments: a simple guide. Society for the Preservation of Natural History Collections (SPNHC) leaflet 1(1), 1-4. Available from www.spnhc.org.

Chidichimo, G., Dalena, F., Beneduci A., 2015. Woodworm Disinfestation of Wooden Artifacts by Vacuum Techniques. Conservation Science in Cultural Heritage, 15, 267-280.

Daniel, V., Hanlon, G., Maekawa, S., 1993. Eradication of Insect Pests in Museums Using Nitrogen. WAAC Newsletter 15(3),15-19

Gilberg, M., 1991. The Effects of Low Oxygen Atmospheres on Museum Pests. Studies in Conservation , 36, 93-98.

Hanlon, G. , Daniel, V., Ravenel, N., 1992. Dynamic System for Nitrogen Anoxia of Large Museum Objects: A Pest Eradication Case Study. Proceedings of the Second International Conference on Biodeterioration of Cultural Property, Oct 5-8, 1992, Yokohama, Japan.

Jian, F., Jayas, D.S., White, N.D.G., Fields, P.G. and Howe, N., 2015. An evaluation of insect expulsion from wheat samples by microwave treatment for disinfestations. Biosystems Engeneering, 130, 1-12.

Jiao, S., Tang, J., Johnson, J. A. and Wang, S., 2012. Industrial-scale radio frequency treatments for insect control in lentils. Journal of Stored Products Research, 48, 143-148.

Jiao, S., Tang, J., Johnson, J.A., Tiwari, G. and Wang, S. 2011. Determining radio frequency heating uniformity of mixed beans for disinfestation treatments. Transaction American Society of Agricultural and Biological Engineers, 54, 1847-1855.

Kelen, A., Ress, S., Nagy, T., Pallai, E., Pintye-Hodi, K., 2006. Mapping of temperature distribution in pharmaceutical microwave vacuum drying. Powder Technology, 162, 133-137.

Koestler, R.,J., 1993. Insect eradication using controlled atmospheres, and FTIR measurement for insect activity. ICOM 10th Triennial Meeting, Washington, D.C. Vol. II, 882-886.Koestler, R.J., 1996. Anoxic treatment for insect control in panel paintings and frames with argon gas.

American Institute of Conservation Paintings Specialty Group, Postprints. AIC, 1717 K Street, NW, Suite 301, Washington DC 20006, 61-72.

Koestler, R.J., 1992. Practical application of nitrogen and argon fumigation procedures for insect control in museum objects. In: Toishi, K., Arai, H., Kenjo, T., Yamano, K. (eds.), 2nd International Conference on Biodeterioration of Cultural Property, Yokohama, Japan, 5-8 Oct 1992, 94-96.

Lewis, V.R. 1997. Alternative Control Strategies for Termites. Journal of Agricultural Entomology, 14, 291-307.

Lewis, V.R. and Haverty, M.I. 1996. Evaluation of Six Techniques for Control of the Western Drywood Termite (Isoptera: Kalotermitidae) in Structures. Journal of Economic Entomology, 89, 922-934.

Nelson, S.O. and Trabelsi, S. 2012. Factors influencing the dielectric properties of agricultural and food products. Journal of Microwave Power and Electromagnetic Energy, 46, 93-107.

Pan, L., Jiao, S., Gautz, L., Tu, K. and Wang, S., 2012. Coffee been heating uniformity and quality as influenced by radio frequency treatments for postharvest disinfestations. Transaction American Society of Agricultural and Biological Engineers, 55, 2293-2300.

Plaza, P.J., Zona, A.T., Sanchís, R., Balbastre, J.V., Martínez, A., Muñoz, E.M., Gordillo, J., de los Reyes, E, 2007. Microwave Disinfestation of Bulk Timber. Journal of Microwave Power and Electromagnetic Energy, 41, 22-37.

Selwitz, C.,and Maekawa, S., 1998. Inert gases in the control of museum insect pests. The Paul Getty Trust, (USA), 1998.

Shayesteh, N. and Barthakur, N. ,N., 1996. Mortality and behaviour of two stored-product insect species during microwave irradiation. Journal of Stored Products Research, 32, 239-246.

Strang, T.,K., 1995. The effect of thermal methods of pest control on museum collections'. In: C. Aranyanak and C. Singharsiri (eds.) Biodeterioration of Cultural Property 3, Bangkok 1995), Office of Archaeology and National Museums, Bangkok, 334-353.

Strang, T.,K.,J., 1992. A review of published temperatures for the control of pest insects in museums. Collection Forum, 8(2), 41-67.

Unger, A., Schniewind, A.,P., Unger, W., 2011. Conservation of wood artifacts. A handbook. Chapter 8, , Springer-Verlag, Heidelber, Germany, 285-289.

Vivancos-Ramon, V., Perez-Marin, E., Nuno-fernandez, L., Balbastre-Tejodor, J.,V., Zona-Ortiz, A.,T., 2006. Microwave treatment for woodworm disinfection in large format works of art. In: R. Fort, M. Alvarez del Buergo, M. Gomez-Heraz, and C. Vazquez-Calvo eds, Heritage Weathering and Conservation, Talylor & Francis Group, London, UK.

Wang, S., Tiwari, G., Jiao, S., Johnson, J.,A., Tang, J., 2010. Developing postharvest disinfestations treatments for legumes using radio frequency Energy. Biosystems Engeneering, 105, 341-349.

Chapter 3

Woodworm disinfestation of wooden artefacts by vacuum techniques

Abstract

As seen in Chapter 1 and Chapter 2, the wood is subject to being damaged by various types of biological infestation (i.e. bacteria, insects, fungi, etc) that cause loss of the chemical and physical properties of wood. As seen in Chapter 2, one of the major causes of deterioration is due to infestation of the wood by wood-eating insects (woodworm larvae). These larvae tend to feed the cellulose and the starch content in the wood, creating canals within this leading inevitable loss of its mechanical properties (with a consequent embrittlement).

Also in this part of this PhD research work it was devoted precisely to the disinfestation of wooden artefacts trying a method that is safe for both the sample in analysis, both for the operator that deals of the maintenance and restoration of wooden artefacts. In fact, most of disinfestation techniques involve the use of extremely toxic substances such as SO_x and NO_x. In this experimental work we were conducted experiments for efficient disinfection by dehydration of the parasite (the case was studied on more coriacea species of larvae: the *Hylotrupes bajolus*). In the case of this experimental work, the dehydration was induced in vacuum conditions.

Chidichimo, G., Dalena, F. , Beneduci, A., 2015. Woodworm disinfestation of wooden artifacts by vacuum techniques, Conservation Science in Cultural Heritage 15(1), 267-272

3.1. Introduction

As it can be seen in the previous chapter, during the larval stage, the worm uses the cellulose contained in the wood to nourish itself and as a consequence bores deep tunnels through the wooden artifact, destroying the mechanical performance of the material. This problem, in the large majority of conservative interventions, is solved by exposing the artifact to chemicals which, in the case of accidental spillage, can be dangerous for workers performing conservation operations. These methodologies have the further inconvenience of not being very effective in destroying the insects' eggs.

Methods used for woodworm disinfestations can be classified into two major categories: chemical and non-chemical. A detailed comparison of the most widely used methods for controlling woodworm attacks can be found in the works of Lewis and Haverty (1996). Chemical products that must be directly applied to the wood, include pyrethrum aerosol and pyrethroid aerosols and liquids (cyluthrin, permethrin, bifenthrin) liquid imidacloprid, liquid nitrogen, and liquid and powder formulations of disodium octaborate tetrahydrate (Plaza et al., 2007).

All these substances have to be carefully handled by trained operators for the reasons mentioned above. As a result, there is growing interest in non-chemical insect control. Non-chemical treatments for wood disinfestation include heat (lethal levels - above 53 ºC- for at least 33 minutes - are used on the wooden artifacts ensuring the death of the parasites (Lewis, 1997); this method however, can damage the wooden artifacts), electrocution (based on high voltage-low current devices) with effectiveness as low as 44% (Lewis, 1997) and microwave (MW) irradiations (Chidichimo et al., 2017).

This paper describes a new technique of disinfestation based on the possibility of producing irreversible damage to worms by creating vacuum conditions around the artifact. The aim of this study therefore was to find a useful protocol for worm disinfestation by vacuum and more precisely, to find the minimum vacuum treatment time for complete disinfestation of walnut wood (*Liquidambar styraciflua*) from *Hylotrupes bajolus* larvae.

To our knowledge, no experiments have been made regarding this argument. Today, creating a vacuum around an artifact does not seem to be a complex matter and is an interesting way to ascertain the possibility of worm disinfestation as the methodology avoids the use of harmful chemicals, physical heat or electromagnetic radiation treatment, which can produce wood dehydration.

3.2 Experimental

The apparatus used to perform the vacuum experiments is illustrated in Figure 3.1. This was essentially constituted by a spherical dessicator made in Plexiglas, thick enough to withstand a gradient pressure of more than 1.2 atm between the external and internal surfaces, connected to an Edwards rotary vacuum pump able to create a vacuum of 10^{-2} atm, and an appropriate pressure gauge.

Figure3.1. *Apparatus used to perform vacuum experiments*

In order to perform a significant number of experiments it was necessary to breed *Hylotrupes bajolus* larvae by choosing as an incubator chestnut wood already infested with worms. Infested chestnut wood trunks (with an average diameter of 10 cm) were kept for 9 months at a temperature of 20°C with a relative humidity level of 70% in suitable ventilated containers. These environmental parameters allowed optimal growth of a sufficient number of larvae to carry out our experiments. Figure 3.2 shows a *Hylotrupes Bajolus* larva.

Figure 3.2. *Hylotrupes Bajolus larva*

Preliminary experiments were conducted on larvae extracted from their natural environment (i.e. the wood where they were bred) and placed in isolation in the apparatus shown in Figure 1. They were then exposed to a vacuum of 10^{-2} atm. The experiment showed that the larvae are able to maintain their viability for a few hours in these vacuum conditions. Only after more than 10 hours treatment, the worms, in their larval state, lost their mobility and appeared to be smaller in diameter. We therefore concluded that under vacuum conditions, worms gradually lose water and become progressively dehydrated. Worms that were kept isolated moreover, were no longer able to rehydrate themselves to regain their viability. At this stage we were unable to answer the following question: did worms that were kept in their natural habitat and subjected to vacuum conditions inside their tunnels behave in the same way as isolated worms, or could they rehydrate themselves by retrieving water from the wood? In other words, we were unsure whether the conclusion regarding the worms extracted from their natural environment could be assumed valid for the worms left in their habitat, as is the case for larvae-infested artifacts, without any further evidence. Worms inside the wood could indeed rehydrate themselves by taking moisture from the wood by mechanisms of diffusion or simply feeding on the cellulose.

Another problem to solve was to find measurable parameters which would indicate worm death.

Our conclusion was that in order to solve these problems, experiments would need to be conducted leaving the larvae inside their natural habitat and measuring a number of parameters linked to their activity to ascertain their viability. To this end, the larvae contained in the pieces of chestnut wood where they had been naturally bred were subjected to vacuum conditions. All chestnut wood testing samples were of a cylindrical shape measuring 5 cm in height and with a diameter of about 10 cm. Each of them contained a single worm nested in the area between the bark and the dead wood. In

order to follow the viability of the larvae in the course of the vacuum treatment we opted to measure the quantity of waste powder produced by the worm during its eating activity. This waste material can be easily collected by simply tapping the cortex of the wood cylinder next to the open cavity created by the worm, placing the sample with the cavity face down. A sample used in the experiments (sample N.7), as well as the waste powder produced by the worm at certain stages of the experimentation is shown in Figure 3.3.

Figure 3.3. *One of the samples used in the experiments*

The cavity produced by the larva is clearly visible on the left side of the sample. The waste powder extracted by the procedure described above is also shown.

Experiments were carried out on control samples, where larvae were left undisturbed, and samples submitted to 8, 24, 120 and 140 hours of vacuum treatment at a pressure of 10^{-2} atm. For each of these conditions three samples were tested in order to reduce experimental error. The waste powder was collected and weighed at given time intervals. Overall research time was 35 days for each sample. From now on, the waste powder produced by the worms will be referred to as WP for brevity.

3.3. Results and discussion

WP produced by the worms' feeding activity during the vacuum experiments are reported in Figure 3.4. At the beginning of the experiments, each of the samples was cleaned by removing all the WP produced until then by the hosted worm. On each of the days corresponding to the experimental

points reported in the graphs in Figure 3.4, the accumulated WP was removed from the samples, then weighed. The result corresponds to the WP produced in the interval between the actual and previous measurement of the day before. The weight of this WP was then added to the previous one. The vacuum treatment started on the 9th day of experimentation in all of the cases, as indicated by the black arrow in Figure 3.4.

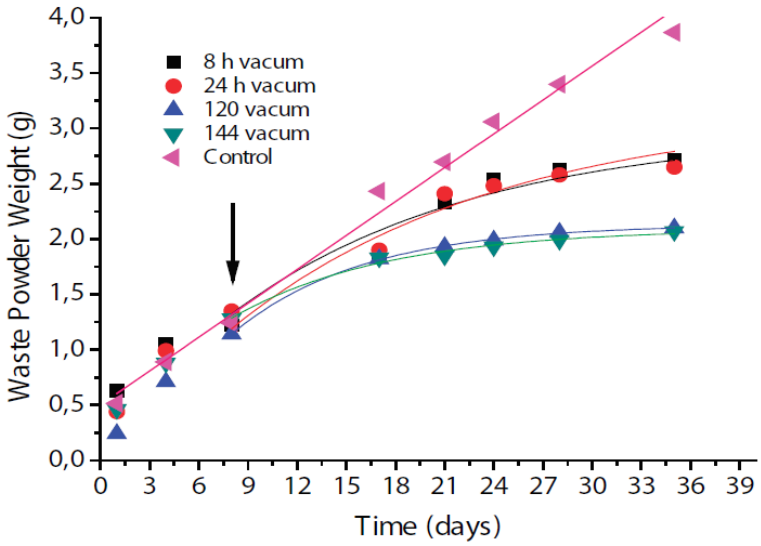

Figure 3.4. *WP produced by the worms as a function of days, for four different vacuum times (hours) treatments and for the control sample that was not vacuum treated. Points corresponding to each of the trends represents the average WP quantities measured from the activity of three different worms (see text). The vacuum treatment started on the 9th day, indicated by the black arrow.*

First of all, it is interesting to note that the total amount of WP produced by the control worm samples follows an almost linear trend from the beginning to the end of the experiments. The slope is 0.10 grams/day with a margin of error of about 4%. This means that the eating rate of the control worms remains constant and is not affected by manipulation of the samples during the WP collecting procedure. In the other cases, before vacuum treatment, the slope of the WP accumulation remains very close to that of the control, while after treatment, the WP accumulation loses the linear trend to assume an exponential one. This is clearly seen in Figure 3.4 where the linear fit for the control and the exponential fit for the vacuum treated samples are reported as continuous lines. The exponential fit is described using the following equation:

$$WP = WP_{\infty} + Ae^{-kt} \qquad (7)$$

Where, *WP* is the cumulative waste powder produced at the time t, *WP*∞ is the cumulative waste that would be produced at infinite time, *k* is the kinetic constant of worm degradation expressed as days-1 and A is a pre-exponential factor which is related to the starting WP accumulated at the time of vacuum treatment.

The fitting results are reported in Table 3.1.

Sample	**WP_∞**	**K**	**R^2**
8h	3,17274 (±0,438)	0.06 (±0.03)	0,949
24h	2,98241 (±0,393)	0.07 (±0.03)	0,928
120h	2,09386 (±0,059)	0.106 (±0.022)	0,980
144h	2,13252 (±0,012)	0.125 (±0.005)	0,999

Values in parenthesis are standard deviations of the data

Table 3.1. *Exponential Fitting results of the WP data of vacuum treated worms shown in Figure 3.4*

It is interesting to note that the metabolic activity of the worms does not stop abruptly with the beginning of the vacuum treatment (Figure 3.4), but gradually decreases to zero in an exponential trend. The kinetic constant of this trend gradually increases as the vacuum time increases, as shown in Table 3.1. We can assume that this constant represents the rate of worm degradation induced by the vacuum treatment. Therefore, the longer the treatment, the faster the degradation. This is also reflected in the rate at which the WP reached infinite value. This was indeed reached after about 15 days from treatment in the cases of the 120 h and 144 h samples (5 and 6 days of vacuum treatment, respectively) while, only after about 25 days in the other cases (0.3 and 1 day of vacuum treatment). In addition to the waste production analysis, at the end of the experiment, we observed each of the treated worms and found that all of the worms examined had died as a result of the significant dehydration caused by the vacuum treatment.

3.4 Conclusion

Summarizing the results, we have shown that for a vacuum time of the order of 8 hours, worms stop their activity completely after about 25 days post treatment. For the longer vacuum time treatments of 120 and 144 hours (5 and 6 days) worm activity stops after about 10 days from treatment. Moreover, visual inspection of the worms at the end of the experiments, enabled us to verify that their death had been brought about by dehydration induced by vacuum.

Therefore, we can conclude that 8 hours of vacuum treatment at 10^{-2} atm are enough to disinfest wood artifacts from *Hylotrupes bajolus.* Although worms will continue their activity for some time after they have been exposed to the vacuum, the biological damage caused to them during the treatment is irreversible and ultimately leads to the worms' death.

This appears to be a very promising technique, since it does not expose operators to any chemical or physical risk.

References

Lewis, V., R., 1997. Alternative Control Strategies for Termites. J. Agric. Entomol., 14, 291-307.

Lewis, V. R., and Haverty, M., I, 1996. Evaluation of Six Techniques for Control of the Western Drywood Termite (Isoptera: Kalotermitidae) in Structures." J. Econ. Entomol., 89(4), 922-934.

Plaza, P.,J., Zona, A.,T., Sanchís, R., Balbastre, J.,V., Martínez, A., Muñoz, E.,M., Gordillo, J, and de los Reyes, E., 2007. Microwwave Disinfestation of Bulk Timber. Journal of Microwave Power & Electromagnetic Energy, 41 (3), 22-37.

Chidichimo, G., Dalena, F., Rizza, A., Beneduci, A., 2017. Wood disinfestations from larval *Hilotrupes baiolus* by microwave radiation: effects on wood dehydration. Studies in Conservation, IN PUBBLICATION

Part 2

New methods for ancient book de-acidification

This part of thesis, concerns a new method to recover book acidity and some new insight regarding surface electrode pH measurements. In particular chapter 4 "*De acidification of ancient books: technique and experimental results*" reports the results obtained in book de-acidification by using an original aerosol technique. During this part of the work we become aware that pH measurements made on paper by surface contact glass electrode suffered by which affected the measurement reproducibility. We decided to investigate this phenomena and to bring it at a final explanation. In chapter 5 "*Paper pH detection by surface electrode: a model to explain the time evolution of ph values during measurements*" we report the results of such an analysis.

Chapter 4

De acidification of ancient books: technique and experimental results

In this part of the work it is tested a testing based on the use of the aerosol system that allows the deposition of a basic solution of books not de paged. This trial provides that the experiment is conducted under vacuum conditions. The deposition of micro-droplets sprayed at a high pressure in the vacuum condition pages, allow a deacidification of the paper in analysis. In particular it has been tried to develop a new technique to de-acidify multiple volumes simultaneously, without the need to de-paging of books and their immersion in solutions that could irreversibly affect their appearance and their mechanical resistance ensuring low cost and speed of treatment.

4.1 Introduction

Cellulose (as discussed in Chapter 1) is a simple polymer composed of linear β-1,4-linked D-glucopyranose chains (also called glucose or glucan chains). While β-1,4-linked glucose is the chemical repeating unit, the structural repeat is β-cellobiose (Varrot et al., 2003) In cellulose, glucose chains are tightly bound to each other by van der Waals forces and hydrogen bonds into crystalline structures called elementary fibril (consisting of around 40 glucan chains), about 40 Å wide, 30 Å tick and 100 Å long (Bidlack et al., 1992). Aggregates of elementary fibrils, of essentially an infinite length, and a width of approximately 250 Å, are called microfibrils (Fan, et al., 1982). Regions within the microfibrils with high order are termed crystalline, and less ordered regions are termed amorphous. The term “amorphous” cellulose is widely accepted even though it can be contradictory. Amorphous material is defined as material which is formless or lacks definite shape, however, amorphous cellulose probably still possesses some degree of order (O’Sullivan, 1997). Larsson, et al. (1997), investigated molecular ordering of cellulose and reported that most of the amorphous regions correspond to the chains that are located at the surface, whereas crystalline components occupy the core of the microfibril, Fig. 4.1.A. A different molecular architecture of

crystalline and amorphous cellulose is suggested by Moiser et al. (1999) and Tenkanen et al. (2003). They describe cellulose as being semi-crystalline, with regions of high crystallinity averaging approximately 200 glucose residues in length separated by amorphous regions, Figure 4.1.B.

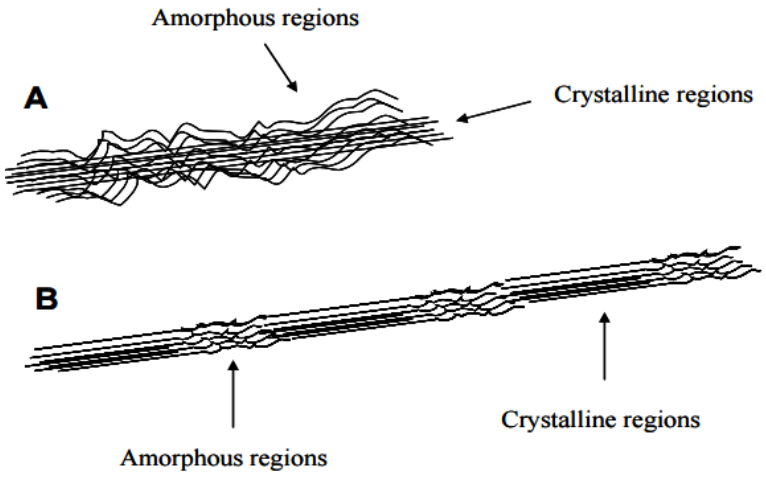

Figure 4.1: *Two different views on how crystalline and amorphous cellulose is distributed within the microfibril. A: Crystalline cellulose is in the core of the microfibril, and it is surrounded by amorphous substrate. B: Crystalline and amorphous regions are being repeated in horizontal dimension .*

Native cellulose has the degree of polymerization (DP) up to 10.000 β- anhydroglucose residues (Hon and Shiraishi, 1991). This means that the molecular weight is above 1.5 million [g/mol]. As the length of the anhydroglucose unit is 0.515 nm (5.15 Å), the total length of the native cellulose molecule can reach 5 µm.

The amorphous zone make cellulose more easily exposed to degradation phenomena such as chemical degradation (hydrolysis) and oxidation.

The hydrolysis consists in the breakage of the glucosidic bond between the various molecules of monosaccharide, from which it follows the formation of fragments that determine the decrease in the degree of polymerization of the chain. Consequently, the reduction of the length, leads to a lower strength of the paper.

The hydrolysis of the glucosidic bond can be either type of acid or basic type. In particular, the acid hydrolysis is a more frequent degradation phenomenon since the catalytic activity of the reaction occurs even at low temperatures (Bettolo, 2007).

The acid hydrolysis is a two steps reaction. The "protonation", ie the sum of an ion H_3O^+, coming from the dissociation of 'acid, to the oxygen atom involved in the glucosidic bond. This involves the formation of a positive charge on the oxygen atom, which promotes the addition of H_2O molecule at one of the two carbon atoms involved in the glucosidic bond protonated that subsequently releases the proton. (Fig. 4.2) (Blazej, A., and Kosik, M.,1985).

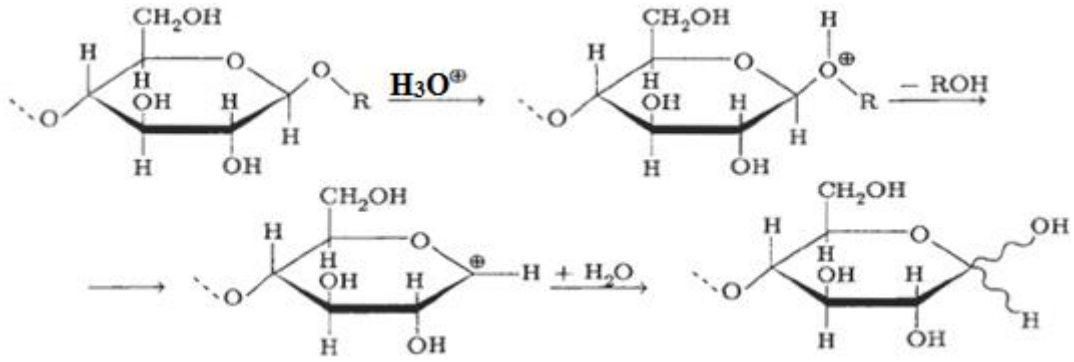

Figure 4.2. *Acid hydrolysis of cellulose.*

A strongly alkaline environment, in conditions of high temperature (above 150 ° C), can also cause hydrolysis and degradation of the polymeric structure. In this case, the deprotonation of the hydroxyl at C (2) form a reactive species (ion alkoxide), intramolecularly so nucleophile that attacks the anomeric carbon, thus causing the detachment of the alcoholic part of the glucoside (Fig. 4.3).

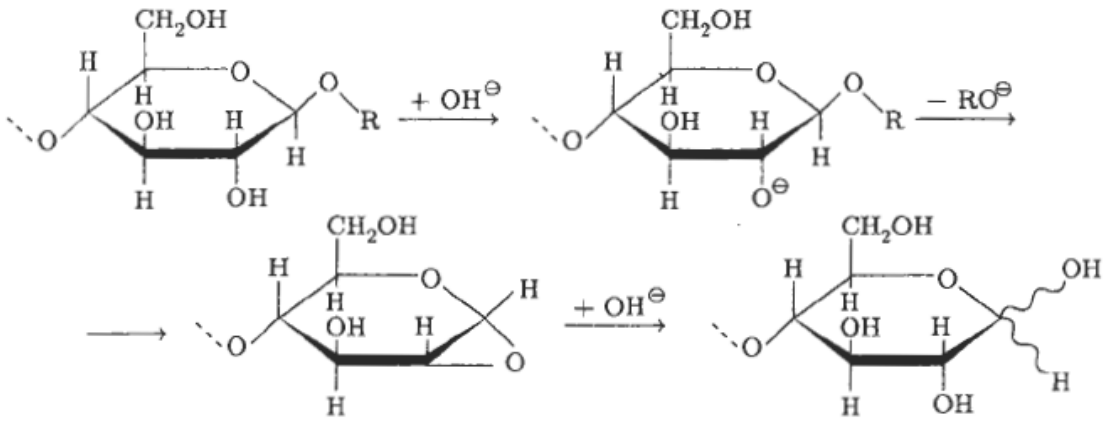

Figure 4.3. *Alkaline hydrolysis of cellulose.*

This hydrolytic cleavage can occur randomly, that is, at every point of the chain. In an alkaline environment can be further degradative hydrolysis, known by the name of *peeling off* (Fig. 4.4) (Sarybaeva et al., 1991). It also takes place at temperatures below 100 °C. In the alkali, the reducing end (the terminal glucose) of the cellulose molecule, isomerizes, through the ene-diol form, the corresponding ketose, on which a reaction takes place of β-elimination . If the β-elimination occurs at the level of the C (4), there is output of the remainder of the chain (Beckwith et al., 1940; Allsopp et al., 2004).

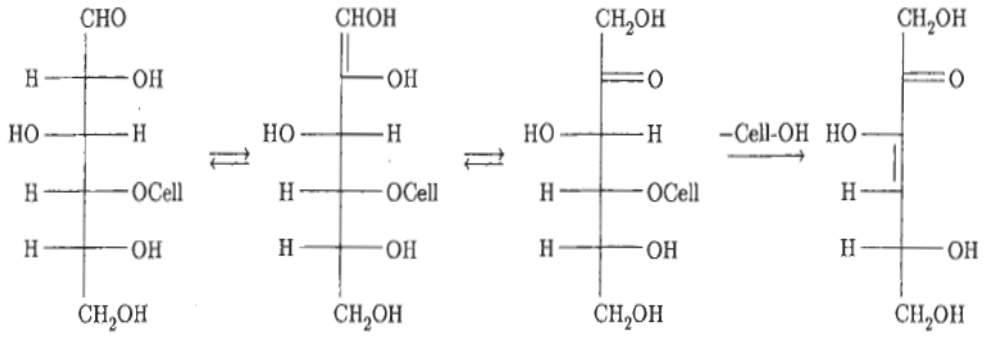

Figure 4.4. *Degradation of cellulose by alkaline peeling off.*

The ketose residue undergoes further transformation to isosaccaric acid. The reaction is repeated on the new reducing ends of the chain, then the degradation occurs with the detachment of a unit at a time, hence the name of the process. In general, occurred the detachment of approximately 50 units, the reaction of peeling off is blocked for the intervention of the process of termination reactions, in which it has a β-elimination of different carbon atom from the C (4), and the end reducing agent is converted to benzyl rearrangement in stable metasaccarinic acid in alkaline environment (Baty et al., 2010). In general, the processes of alkaline hydrolysis are more uniform than those of acid hydrolysis because the alkaline solutions have a high swelling capacity in respect of the cellulose, and therefore the crystallites are more accessible than they are in an acid environment. The hydrolytic processes cause a decrease of the degree of polymerization which can be assessed by measurements of viscosity and also measures the change in the reducing power, to increase the number of terminal aldehyde groups.

4.2 Experimental

For the realization of the treatment prototype was built a vacuum chamber composed of two vacuum dryers of equal size (denoted with the numbers “2” and “3” in the Figure 4.5) linked by a special vacuum tube equipped with a stopcock. The two dryers have been connected, one to a vacuum pump *Edwards II GT 3(*denoted with the number “1” in the Figure 4.5*)*, while the other to an atomizer *241 Ultra Sonic particle generator* (denoted with the number “4” in the Figure 4.5) by means of which it was possible to atomize a basic solution of $Ca(OH)_2$ 0.05M.

Figure 4.5. *Experimental system for the de-acidification of books in vacuum conditions and aerosolized by dispersion of calcium hydroxide. A pump (1) is connected to a vacuum desiccator (2)with vacuum tubes (the pressure is constantly monitored by a pressure gauge applied between the pump and the dryer). To the first dryer it has been applied a second (3) in turn connected to an atomizer (4).*

While desiccator "2" is placed the sample (the book), there is leads to vacuum condition equal to 10^{-4}atm (pressure read by the pressure gauge applied between the pump and the dryer), desiccator "3" is entered the basic solution of $Ca(OH)_2$ 0.05 M in nebulizer form. The solution was atomized through a 241 Ultra Sonic Particle generator (2.4 mHz) Once saturated with the atomized solution, the "3" dryer is isolated from the atomizer and is opened the tap placed in contact with the dryer "2" where it is contained the sample. Being of equal size, the pressure on the "2" ball and "3" will then be about 10^{-2} atm (less considering the volume of the tube that connects the two dryers). Furthermore, the $Ca(OH)_2$ atomized solution will fill the "2" dryer where is contained the sample.
The purpose of this system is to neutralize the acid pH of the book with a strongly basic solution without damaging for the book. In fact, the basic solution in the form areosolic and under room

temperature conditions, does not catalyzes the reaction of basic hydrolysis harmful for cellulose and inks (as seen in section *4.1 Introduction*). Moreover the low vacuum conditions created guarantee better uniform absorption throughout the sample.

The experimentation was carried out first on a single sheet of paper acidified with a weak acid solution (CH_3COOH 0.005 M) and subsequently on a sample book with an acid pH (a book entitled: *Sixth International Symposium on Surfactants in Solution (1986)).*

The sample was placed in the desiccator "2" and in the case of the book, opened (as shown in Fig.5.6) so as to facilitate the penetration of the aerosol solution between the various pages.

Figure 4.6. *Book sample introduced inside the dryer "2"*

A single application provides the consumption of 50 cc of $Ca(OH)_2$ and a contact time of the basic solution with the sample of 3-hour under vacuum conditions. The total applications for an experimental cycle are five for a total consumption of solution equal to 250 cc. At the end of the experimental cycle the sample was maintained in vacuum conditions for 24 hours.

4.3 Results and discussion

Experimentation on a single sheet of paper

The pH of the single sheet of paper was measured before and after treatment of deacidification (as described in the section *5.2 Experimental*). The experimentation was carried out for one sample that have been made with two treatment cycle that included the consumption of 250 cc of the $Ca(OH)_2$. The samples were stored at the end of each treatment under low vacuum condition for 24

hours (10^{-2} atm). The pH measured before and after the deacidifying treatment, was measured in the same five points, as indicated in Figure 4.7.

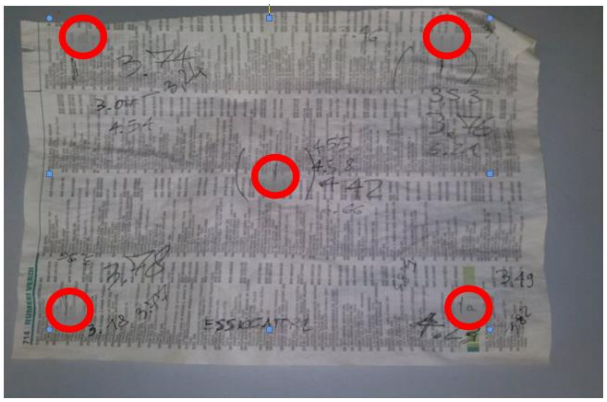

Figure 4.7. *The sample used in this experimentation. In red have been highlighted the five measurement points for each page.*

The results of deacidification treatments are shown in tab.4.1.

Area Analysis	*pH_0*	*pH(1)*	*pH(2)*
1	*3.04*	*5.54*	*6.973*
2	*3.18*	*4.96*	*5.958*
3	*4.08*	*6.67*	*6.954*
4	*3.53*	*6.216*	*6.343*
5	*3.82*	*5.855*	*6,123*

Tab.4.1 *pH values measured on the five points of the sheet before the deacidification treatment, after the first treatment for de-acidification (pH (1)) and after the second treatment of deacidification (pH (2))*

with *pH_0* is defined the pH value before treatment and with *pH(1)* is defined the pH value after the first treatment cycle and *pH (2)* is defined the pH value after the second treatment.

The pH values after the treatment lead to very satisfactory values (the pH reaches neutral values) that confirm the validity of the experimental methodology.

Experimentation on the entire book

It is chosen a sample book with an acid pH. The pH was measured using a surface electrode by at HANNA- Leather & Paper HI 99 171; pH meter with glass electrode surface. The book used as the sample was: *Sixth International Symposium on Surfactants in Solution (1986)*. For pH

measurements were made on nine sample pages (3, 43, 73, 103, 153, 204, 248, 307, 357). five measurements were made for each of these pages: the upper right corner, the upper left corner, lower left corner, lower right vertex and the center of the page as shown in Fig.4.8.

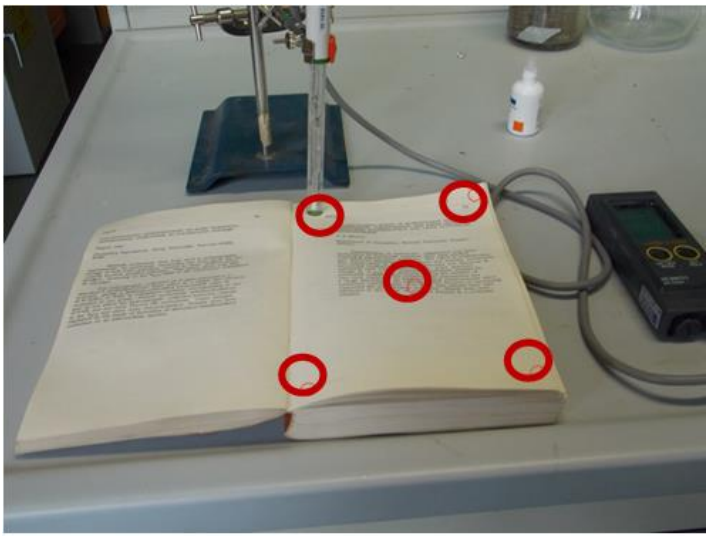

Figure 4.8. *Example of how the measurements were made. In red have been highlighted the five measurement points for each page.*

Measurements were made by placing the electrode on the surface of the sample after applying the *electrolyte conductive solution* (HANNA HI70960). Measurements of pH in standard condition have been made by placing a polypropylene plastic sheet beneath the investigated page. The pH was measured when the pH meter recorded a value defined "stable". They were performed 4 different treatments each of which has had a total consumption of $Ca(OH)_2$ equal to 250 cc. Moreover, the sample was maintained under vacuum conditions (about 10^{-2} atm) for 24 hours for each treatment cycle. The results are shown in tab.4.2. The pH_0 values refer to measurements without treatment cycles. The values of pH(1), pH(2), pH(3) and pH(4), refer to the values measured after respectively one, two, three, four treatment cycles.

	Pag.3	*Pag.43*	*Pag.73*	*Pag.103*	*Pag.153*	*Pag.204*	*Pag.248*	*Pag.307*	*Pag.357*
pH_0	4,914 (±0,297)	4,788 (±0,116)	4,594 (±0,08)	4,612 (±0,057)	4,564 (±0,093)	4,516 (±0,114)	4,658 (±0,068)	4,67 (±0,058)	4,664 (±0,071)
pH (1)	5,03 (± 0,158)	4,848 (± 0,1)	4,788 (±0,134)	4,786 (± 0,115)	4,832 (± 0,14)	4,696 (± 0,108)	4,896 (± 0,066)	4,944 (± 0,092)	4,942 (± 0,069)
pH (2)	5,112 (± 0,169)	5,012 (±0,108)	5,084 (±0,138)	4,984 (±0,104)	5,014 (±0,135)	4,984 (±0,103)	5,14 (±0,06)	5,126 (±0,083)	5,06 (±0,062)
pH (3)	5,39 (±0,158)	5,478 (±0,1)	5,578 (±0,134)	5,386 (±0,115)	5,422 (±0,140)	5,142 (±0,104)	5,546 (±0,066)	5,744 (±0,092)	5,222 (±0,069)
pH (4)	5,89 (±0,158)	6,03 (±0,102)	6,14 (±0,131)	5,944 (±0,118)	6,012 (±0,14)	5,928 (±0,1)	5,896 (±0,066)	6,124 (±0,092)	5,742 (±0,069)

Tab.4.2 A*verage of the pH values measured on nine pages of the book in the analysis. pH (1), pH (2), pH (3), pH (4), refer to the pH measurements after the number of treatments indicated in brackets. The values were averaged over five points measured on each page. the values in brackets are the standard deviations.*

As can be seen from Table 5.2, the results show an efficacy of deacidification treatment.

The pH rose by an average of 0.2 0.19 in the first two treatments (pH (1) and pH (2)) and 0.56 in the third treatment (pH (3)). at the end of 4 cycles of treatment (pH (4)), the average pH of the book is to be equal to 5.95 with values of 6.14 and 6.12 for the pages 73 and 307 respectively. These values are corresponding to pH values safe for the degradation of cellulose.

Comparison of the experimental values

The average of the pH of the results obtained (Tab.4.1 and Tab.4.2) are exposed in Tab.4.3.

Number of Treatments	*pH (single sheet)*	*pH (entire book)*
0	*3,53(±0,432)*	*4,664 (±0,121)*
1	*5,844 (±0,646862)*	*4,862 (±0,101)*
2	*6,466 (±0,471)*	*5,057 (±0,061)*
3	/	*5,434 (±0,182)*
4	/	*5,967 (±0,124)*

Tab.4.3 *Average of the pH values obtained in Tab.5.1 and in Tab. 5.2*

The results of tab.4.3 were plotted in Fig.4.9.

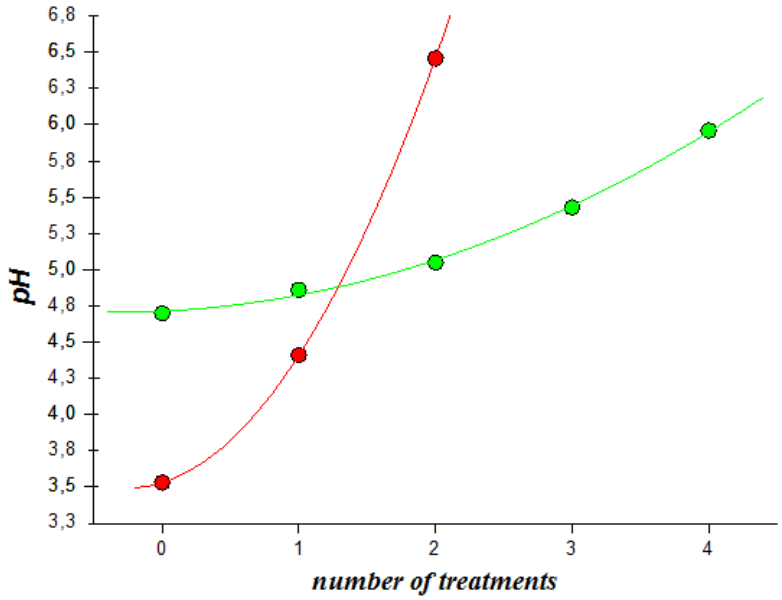

Figure 4.9. *Average values of pH in function of the numbers of treatments. In red are present the data for the testing of single sheet; in green values for the testing of the entire book*

It is easily deduced from the graph that the pH reach the neutrality much faster then the case of the experimentation on single sheet of paper (in red in the Fig.4.9) compared to the values obtained for the entire book experimentation (in green in the Fig.4.9). In both cases they were obtained pH values not damaging for the paper, but, in the first case the pH reaches an average value of about 6.5 with only two cycles of treatment, while for the experiment with the entire book is reached a value of about 6.0 with four treatment cycles. This is perfectly justified by the fact that the book presents a comprehensive paper surface of at least three hundred times higher (the number of pages of the book is 365) with respect to the paper sheet. The same amount of base solution that was administered to a single sheet of paper, was dispersed instead of 365 pages in the case of the book. A much weaker increase of pH in the case of the book, the order of magnitude observed was totally expected.

4.4 Conclusion

It is demonstrated that, to neutralize the pH of acid paper, is not necessary to immerse in a liquid solution after having de assembled into individual pages, as practiced in most of the restoration interventions until now used, but it may be sufficient to use a basic solution in the form of micro aerosol droplets administered under vacuum conditions on the texts do not de-assembled.

The results obtained and shown in Table. 4.1 Tab.4.2 and Tab.4.3, prove it: it was possible to achieve levels of nearly neutral in a few cycles of treatment. The experimental method we have developed is completely new and potentially superior to existing techniques that can be harmful both for the sample, both for the operator. The advantages of the proposed methodology are:

- an optimization of operating times;
- a non-invasive for the artistic heritage;
- a secure deacidification procedure for the operator
- greater operational simplicity.

The technique is still in the stage of further experimentation and can be still optimizable:

Further experimentation that will lead to an increase in the volume of solution consumed and more high vacuum conditions, may lead to a further halving of the operating times that were needed to the neutralization of the power of the book acid making this technique a bulwark of the conservative methods and restoration.

References

Allsopp, D., Seal, K., J., Gaylarde, C., C., 2004. Introduction to biodeterioration. Cambridge University Press.

Baty, J., W., Maitland, C., L., Minter, W., Hubbe, M., A., Jordan-Mowery, S. K., 2010. Deacidification for the conservation and preservation of paper-based works: A review. BioResources, 5(3), 1955-2023.

Beckwith, T. D., Swanson, W. H., & Iiams, T. M. (1940). Deterioration of paper: the cause and effect of foxing. Publ. Univ. Calif., biol Sci., 1(13).

Bettolo, R. M., Migneco, L. M., & Zappalà, M. P., 2007. I materiali cellulosici e le loro materie prime, cap. 7 in Chimica per l'arte. Bologna, Zanichelli, 411-485.

Bidlack J, Malone M, Benson R. 1992. Molecular structure and component integration of secondary cell wall in plants. Proc. Okla. Acad. Sci. 72: 51-56.

Blazej, A., & Kosik, M. (1985). Degradation reactions of cellulose and lignocellulose. Cellulose and its derivatives: chemistry, biochemistry and applications/editors, JF Kennedy et al. (eds.), Ellis Horwood, U.K., 97-118.

Fan LT, Lee Y-H, Gharpuray MM. 1982. The nature of lignocellulosics and their pretreatments for enzymatic hydrolysis. Adv. Bichem. Eng/Biotechnol 23: 158-187.

Hon D N-S, Shiraishi N. 1991. Wood and cellulosic chemistry. New York: Marcel Dekker, inc. 1032 p.

Larsson PT, Wickholm K, Iversen T. 1997. A CP/MAS 13C NMR investigation of molecular ordering in celluloses. Carbohydr. Res. 302: 19-25.

Moiser NS, Hall P, Ladisch CM, Ladisch MR. 1999, Reaction kinetics, molecular action and mechanisms of cellulosic proteins. Adv. Biochem. Eng. Biotehnol. 65: 23-40.

O'Sullivan. 1997. Cellulose: the structure slowly unravels. Cellulose 4: 173-207.

Sarybaeva, R., I., Sultankulova, A., S., Vasilikova, T., V., Afanashev, V., A., 1991. Degradation of cellulose in the presence of Lewis acids. Cellulose chemistry and technology, 25(3-4), 199-210.

Tenkanen M, Niku-Paavola M-L, Linder M, Viikari L. 2003. Cellulase in food processing Iin Handbook of food enzymology. New York: Marcel Dekker Inc. p 879-915.

Varrot ,A., Frandsen, T.P., von Ossowski, I., Boyer, V., Cottaz, S., Driguez, H., Sculein, M., Davies, G.J., 2003. Structural basis for ligand binding and processivity in cellobiohydrolase Cel6A from Humicola insolens. Structure. 11: 855-864.

Chapter 5

Paper pH detection by surface electrode: a model to explain the time evolution of ph values during measurements

Electrochemical measurement of pH on paper artifacts is a very important tool to assess the state of paper conservation. Different methods using different type of electrodes have been standardized to provide reproducible pH values of paper. One of these methodologies is very low invasive since it is made on the paper surface by means of a surface electrode contacting the paper through a small layer of water previously added at the measurement point. This method is very convenient but suffers by the fact that the pH value given by the instrument is continuously changing during the measurement with a very fast rate in the first seconds and tending to reach a plateau value after very long time. Usually, the measure is taken at a time after which the rate of pH change is below a given value, i.e. when the value can be considered constant. This condition is usually signaled by an automatic instrumental alert provided to the operator. This pH value, however, is not the asymptotic one, which can be reached only at infinite time. Here we have investigated this behavior showing that it is simply due to the gradual diffusion of water away from the measurement region under the electrode. A theoretical model, which reproduces very well the time dependence above discussed, has been developed. The validity of the model has been completely proved by taking in consideration experiments were water diffusion is prevented in a simple confining apparatus. This

Chidichimo, G., Beneduci, A., Dalena, F., De Simone, B.,C., Lania, I., Gallucci, M.C., Paper Ph Detection By Surface Electrode: A Model To Explain The Time Evolution Of Ph Values During Measurements, Analitical Chemistry, UNDER REVIEW

work shows that it is possible to eliminate any factor affecting accuracy and reproducibility of pH data of paper measured by the surface electrode method.

5.1 Introduction

One of the major problems in preservation of cultural heritage is to prevent damaging of paper and bookbinding in historic books and manuscripts that can be caused by the effect of aggressive atmospheres, humidity and temperature excursions, alterations of paper constituents and added materials such as ink and hand coloring with pigments or dyes (Faubel et al., 2007). Deterioration of paper-based materials is mainly due to the degradation of cellulose caused by a number of factors (Abdel-Maksoud, 2011). One of the most feared is the chemical attack due to acidic hydrolysis. For this reason, it is necessary to measure paper pH, because it is one of the most important parameters defining its longevity (Strlič et al., 2005).

An early scientific publication relating the measurement of paper pH with a glass electrode in conjunction with a chloride-calomel reference electrode, is that of Herbert F. Launer (1939), who proposed the use of this method for pH measurements of hot extracts from paper, in contrast with the previously used methods of the total acidity. Nowadays there are three different standardized procedures for measurement of paper pH, that make use of pH meters. They are the Cold Extraction (TAPPI T 509 om-02, ASTM D778-97(2002)), Hot Extraction (TAPPI T 435 om-02, and ASTM D778-97(2002)) and the Contact Method (TAPPI T 529 om-99) (TAPPI Test Method T509 om-88, 1992; TAPPI Test Method T435 om-88, 1992.). These TAPPI methods differ on the H_3O^+ extraction process from the paper. The first two methods consist in the extraction of hydrogen ions from a suspension of paper in water at 100 °C and 25°C, respectively, for one hour. The TAPPI Contact Method involves the use of a surface flat electrode (Strlic et al., 2004).

The contact method can be considered almost noninvasive, since pH measurement is simply made by placing the flat electrode surface on the top of a water droplet used for wetting the paper at the point where the measure need to be done. The H_3O^+ ion concentration generated by the reaction of water with the acid sites of the paper is then detected. The method appears to be very simple and convenient but the investigator, experimenter has to deal with the following data interpretation. During the measurement the instrument detects pH values which change quite rapidly immediately after the electrode contact with the wetted surface of the paper and keep growing, with gradually decreasing speed, up to reach a stable value in times of the order of some minute. Some of the instruments inform the experimenter to not take in consideration the pH values measured during the

fast changing phase, giving a message of instability of the measure. Since the pH continues to change even after this warning disappears, the problem is to understand what is the meaning of the pH values gradually seen by the electrodes and which of them is the most suitable to represent the acidity of paper.

This work takes into consideration the physical and chemical mechanisms which generate the continuous drift of pH measured by surface electrodes on paper surfaces. One of the first evidence that came out during this study was that the major physical factor affecting pH measurements, is the diffusion of water on the paper surface during the measurement time. Experiments have been made in two different conditions: according to the standard TAPPI method, i.e., allowing water to diffuse and in absence of water diffusion, according to the set up described in the experimental section. As we will see, the time evolution of the measured pH is completely different in the two cases. Notably, the asymptotic values obtained in the two mentioned conditions differ for more than 0.5 pH unit. Moreover, the time evolution of pH, determined in suspension conditions according to the TAPPI T 509 om-02, cold extraction method, is analogous the that observed in absence of water diffusion, if the dilution factor (i.e. the paper/water w/v ratio) is took into account in both the experiments.

A Kinetic theoretical model has been developed, to fit the experimental data obtained both in the presence and absence of water diffusion, taking into account the chemical production of H_3O^+ ions, and water diffusion.

5.2 Experimental

Experiments have been performed on a sacrificial acid book: a copy of conference book reports "XI Congresso Nazionale Di Chimica Inorganica". The pH has been measured by a HANNA-Leather&Paper *HI 99171*" pH meter with surface glass electrode.

Standard pH measurements by surface electrode

Measurements of pH in standard condition have been made by placing a polypropylene plastic sheet beneath the investigated page. On each of the measurement point a small drop of milliQ water, (HANNA HI70960 *conductive electrolyte solution)* has been dripped by the droplet dosing cup bottle. The surface electrode has been then set on the water droplet. Both these operations have been made in rapid succession in a time lower than one second. The experimental set up is illustrated in Fig.5.1.

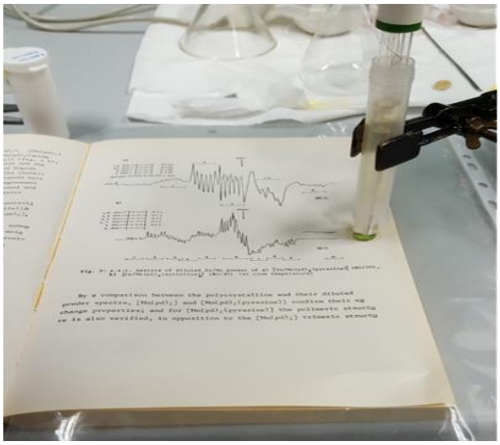

Figure 5.1. *Set up of the pH measurement experiments in standard condition.*

pH values have been registered at intervals of 5 seconds, even during a first time interval of about 30 seconds when the instrument was giving indication that the measure was instable. In actual fact no discontinuity have been observed in the trend of the gradually increasing pH values when the instrument signaled that the measure did enter in the stability regime.

Measurements made by surface electrode in absence of water lateral diffusion

In order to avoid water lateral diffusion during surface electrode pH measurements, disks of paper having the same diameter of the surface electrode, have been used. Each disk has been inserted in a plastic cylinder having a perfectly flat bottom and a diameter of 0.1 millimeters larger than that of the disk (and of the electrode). As in standard measurement a small droplet of water has been added to the paper and measures have been taken by inserting the electrode in plastic cylinder, as it is shown in Fig. 5.2

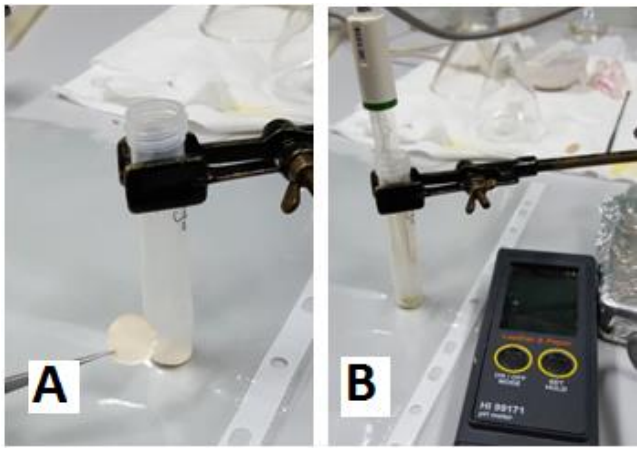

Figure 5.2. *Set up used to perform pH measuerements in absence of water lateral diffusion. A: Plastic cylinder and paper disk sample; B:Electrode insertion into the cylinder to contact the disk and surface water.*

pH measures have been performed as in the standard case.

Measurements made by an immersion electrode (TAPPI cold extraction TAPPI T 509 om-02)

In this case 1.5 grams of paper taken by pages 9 and 12 of the same book used in the experments described above, have been placed in a small becker. A pH meter HANNA HI223 *Calibration Check Microprocessor pH Meter*, working with an immersion glass electrode has been positioned on the top of the paper leaving a space of about 0.1 mm between the paper and the bottom of the electrode. 10 ml of distilled water has been then added and the pH has been measured.

5.3 Results and discussion

The pH values measured according to the standard TAPPI 529 T procedure on three different points of the same sheet of the sacrificial book are shown in Fig. 6.3. It can be noticed that, in every case, the trend of data does not show any discontinuity, despite the fact that the instrument signaled an instability of the measurements in the first thirty seconds after the electrode contact, while indicating a stable regime after this first half minute interval. The only change that can be noticed between these two different regimes is the slope of the data, which goes from a faster growing trend to a slower growing one. It remains open the question on the factors influencing the data evolution.

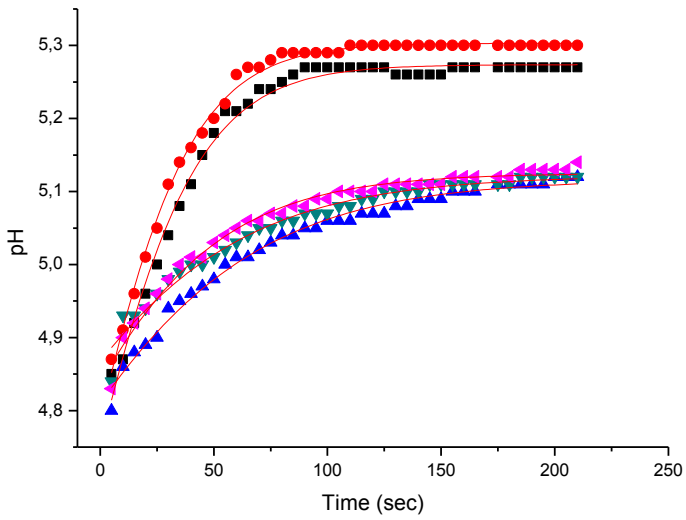

Figure 5.3 *Time variation of pH data made by a surface glass electrode, according to standard procedure. dots black and red are data obtained by different points of pag 24.; dots blue, dark cian, magenta, are data taken from points of page 187.*

A completely different trend has been observed in the case of the measurements made on plastic confined disks (Fig.5.4), where water is not allowed to diffuse laterally with respect to measuring electrode. Indeed, after a fast initial decay, the pH reaches an almost stable value within a time of the order of 30 seconds.

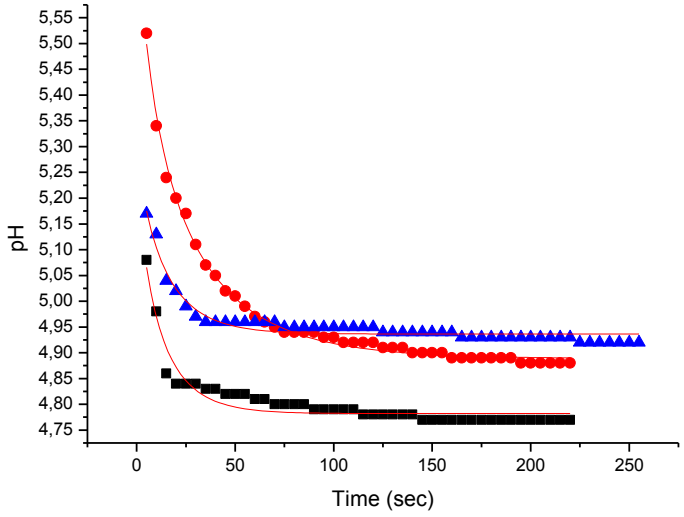

Figure 5.4 *Variation in time of pH data, measured, by a surface glass electrode. Dots black, red and blue are data taken from paper disks cut out from a pages 7, 11, 23 of the sacrificial book(see text) and confined in the bottom of a plastic cylinder to avoid water lateral diffusion.The weight ratio between the paper and the water was 0.60.*

Data taken by the immersion glass electrode, according to the TAPPI T 509 om-02 cold extraction method, are reported in Fig. 5.5. It can be seen that the pH temporal trend is quite similar to that observed in Fig. 5.4. This is not surprising because diffusion of water through the paper cannot have a role on the time evolution of data, being the paper fully immersed in water since the starting of the experiment. The limit values of the time evolution of pH data, of course, shows some substantial differences respect to the analogous limits obtained in the experiments reported in Fig. 5.4, but we will see in the next section that this effect is fully justified by taking into account the different paper/water w/v ratio (dilution factor).

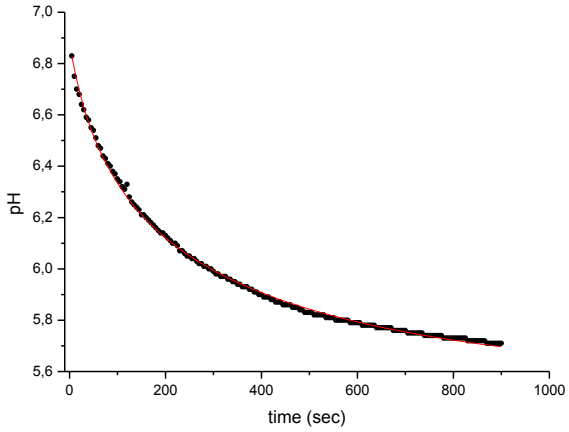

Figure 5.5. *Variation in time of pH data, measured, by an immersion glass electrode. Data are taken from paper, out from a pages 9 and 12 of the sacrificial book(see text). The weight ratio between the paper and the water used in the experiment was 0.15*

In order to explain the trend of data obtained in the two set of experiments above described we developed a theoretical model which takes into consideration both the extraction reaction of H_3O^+ ions by the added water and the lateral diffusion of the water that occurs when standard measurement are performed.

Theoretical model

According to what reported in the experimental section the usual standard measurements of pH on the surface of book pages requires the addition of a small water droplet on the measuring point. This droplet flattens under the electrode surface and then starts to diffuse laterally with respect to electrode expanding the wetted surface in a gradually growing circular region. We hypothesize the occurring of the following reaction in the wetted regions:

$$SH^+ + H_2O \underset{k2}{\overset{k1}{\rightleftharpoons}} S + H_3O^+ \qquad (11)$$

where, SH^+ are the acid sites of the paper being able to generate H_3O^+ ions and S are the conjugate basic sites obtained after hydrogen ion extraction. k_1 and k_2 are the kinetic constants of the direct and inverse reactions. We will call $K= k_1/ k_2$ the equilibrium constant of the reaction 1.

We will also hypothesize that the concentration of SH^+ and S sites, being present on the paper, is much larger with respect to the concentration of H_3O^+ ions generated by reaction 1. This hypothesis seems reasonable when considering that pH values are usually greater than 4, but we are aware that its full justification can be given only when considering the success of the model to reproduce the experimental data. We will show that this is actually the case.

$[SH^+]$ and [S] can be then considered constant, during the evolution of reaction 11, that is to say:

$$[SH^+] = s_a \qquad (12)$$

$$[S] = s_b \qquad (13)$$

Taking into consideration reaction 11, the variation on time of the H_3O^+ concentration can be written according to the following kinetic equation:

$$\frac{d}{dt}[H_3O^+] = k_1 s_a [H_2O(t)] - k_2 s_b [H_3O^+(t)] \qquad (14)$$

The variation in time of the H_3O^+ concentration depends on the variation of the water concentration in the region of the electrode surface. Even if the concentration of water consumed through the reaction 1 is surely negligible, we cannot neglect the variation in the water concentration induced by the lateral diffusion of the water with respect to the electrode surface.

The time variation of water concentration due to the diffusion process can be calculated according the first Fick law:

$$\frac{\partial}{\partial t}[H_2O(\vec{r},t)] = -D\nabla^2[H_2O(\vec{r},t)] \qquad (15)$$

where, D is the diffusion coefficient of water in the paper, when the variation of water concentration due to reaction 11 is neglected. This further approximation is fully justified due to the fact that water concentration remains always much higher with respect to that of H_3O^+ ions. This becomes evident by performing some simple calculation. The moles of water added on the paper are around 10^{-3}. The volume of paper in which this water is absorbed is of the order of 10^{-4} liter. The concentration of water in the wetted paper is than of the order of 10. There is a difference of more than 5 order of magnitude between the water concentration and that of the H_3O^+ ions.

Equation 15 can be solved in two dimensions, since water diffusion along the direction parallel to the electrode axis is prevented by the plastic sheet beneath the paper.

The ∇^2 operator can be conveniently expressed in cylindrical coordinates since both the water droplet placed on the paper beneath the electrode surface and the wetted surface (which gradually enlarges outside from the electrode boundary, during the measuring time) have cylindrical symmetry.

$$\nabla^2 = \frac{1}{\mathrm{r}}\frac{\partial}{\partial \mathrm{r}}\left(\frac{\mathrm{r}\,\partial}{\partial \mathrm{r}}\right) + \frac{1}{\mathrm{r}^2}\frac{\partial^2}{\partial \theta^2} + \frac{\partial^2}{\partial \mathrm{z}^2} \qquad (16)$$

being r, Θ e z, the cylindrical coordinates according to their usual meaning. The water concentration can be taken constant along the paper thickness due to the fact that this thickness is lower than 0.1 millimeter. The wetting process of paper, not only maintains a cylindrical symmetry, but we can further assume that it leads immediately to a uniform distribution of the water concentration along the z coordinate. Then, equation 6 can be simplified as:

$$\frac{\partial}{\partial t}[H_2O(\vec{r},t)] = -D\frac{1}{r}\frac{\partial}{\partial r}\left[r\frac{\partial}{\partial r}[H_2O(\vec{r},t)]\right] \qquad (17)$$

In order to calculate the amount of water in the wetted region under the measuring electrode, eq. 17 can be integrated on the volume of this region:

$$\int_0^L\int_0^{2\pi}\int_0^R \frac{\partial}{\partial t}[H_2O(\vec{r},t)]\,d\tau = -D\int_0^L\int_0^{2\pi}\int_0^R \frac{1}{r}\frac{\partial}{\partial r}\left[r\frac{\partial}{\partial r}[H_2O(\vec{r},t)]\right] r\,dr\,d\theta\,dz \qquad (18)$$

being L the thickness of the page and R the electrode radius. The first member in eq. 18 represents the time derivative of the total quantity of water $(H_2O)_T(t)$ contained in the volume of paper beneath the electrode surface. Once the integration on the coordinates θ and z is performed in the second member of 18, the following result is obtained:

$$\frac{\partial}{\partial t}(H_2O)_T(t) = -2\pi L D\int_0^R \frac{\partial}{\partial r}\left[r\frac{\partial}{\partial r}[H_2O(\vec{r},t)]\right] dr \qquad (19)$$

Integration at the second member of eq. 19 can be easily done as shown below:

$$\int_0^R \frac{\partial}{\partial r}\left[r \frac{\partial}{\partial r}[H_2O(\vec{r},t)] \right] dr = \int_0^R \frac{\partial}{\partial r}[H_2O(\vec{r},t)]dr + \int_0^R r \frac{\partial^2}{\partial r^2}[H_2O(\vec{r},t)]dr =$$

$$\int_0^R \frac{\partial}{\partial r}[H_2O(\vec{r},t)]dr + r \frac{\partial}{\partial r}[H_2O(\vec{r},t)]\Big|_0^R - \int_0^R \frac{\partial}{\partial r}[H_2O(\vec{r},t)]dr = R\left(\frac{\partial}{\partial r}[H_2O(\vec{r},t)] \right)_R$$

Then, we obtain:

$$\frac{\partial}{\partial t}(H_2O)_T(t) = -2\pi L D R\left(\frac{\partial}{\partial r}[H_2O(\vec{r},t)] \right)_R$$

If the two members of the above equation are divided by the volume of the paper lying beneath the electrode ($V = \pi R^2 L$) the time derivative of the water concentration in the region of the glass electrode is obtained:

$$\frac{\partial}{\partial t}[H_2O(t)] = -\frac{2D}{R}\left(\frac{\partial}{\partial r}[H_2O(\vec{r},t)] \right)_R \qquad (20)$$

Equation 20 relates the time derivative of the water concentration in the electrode region with the spatial gradient of the water concentration existing at the electrode contact edge. In order to solve this equation, a specific function for the edge gradient of the water concentration needs to be assumed.

We are guided in this assumption by the following considerations. The edge gradient has its maximum value at the time $t = 0$ (time at which the electrode is put on the water droplet) and reduces to zero for $t = \infty$ (time at which the diffusion process would reduce to zero in absence of other physical phenomena). The exponential function reported below has been chosen as trial function since it has a minimum number of adjustable parameters:

$$\left(\frac{\partial}{\partial r}[H_2O(\vec{r},t)] \right)_R = \varphi_0 e^{-\alpha t}$$

On the basis of this assumption equation 20 can be rewritten as:

$$\frac{\partial}{\partial t}[H_2O(t)] = -\frac{2D}{R}\varphi_0 e^{-\alpha t}$$

to obtain, finally:

$$[H_2O(t)] = [H_2O(0)] - \frac{2D\varphi_0}{\alpha R}\left(1 - e^{-\alpha t}\right) \qquad (21)$$

We have now a specific function of the time for the concentration of water under the measuring electrode. This function can be inserted into equation 14 to calculate the time dependence of the H_3O^+ ions concentration in the electrode region:

$$\frac{d[H_3O^+(t)]}{dt} = k_1 s_a [H_2O(0)] - \frac{2k_1 s_a D\varphi_0}{\alpha R}\left(1 - e^{-\alpha t}\right) - k_2 s_b [H_3O^+(t)] \qquad (22)$$

The mathematical form of equation 22 suggests that its solution must be of the type:

$$[H_3O^+(t)] = \gamma + \beta e^{-\alpha t} \qquad (23)$$

When eq. 23 is substituted into eq. 22 and the time independent terms are collected on the left, while the time dependent terms are collected at the second member, one obtains:

$$\left[k_2 s_b \beta - \alpha\beta - \frac{2k_1 s_a D\varphi_0}{\alpha R}\right] e^{-\alpha t} = k_1 s_a H_2O(0) - \frac{2k_1 s_a D\varphi_0}{\alpha R} - k_2 s_b \gamma \qquad (24)$$

The conditions for which eq.24 holds at any time, are that both the right member and the pre-exponential term on the left must be equal to zero. Under these conditions β and γ are easily calculated:

$$\beta = \frac{2k_1 s_a D\varphi_0}{\alpha R(k_2 s_b - \alpha)} \qquad (25a)$$

$$\gamma = \frac{k_1 s_a}{k_2 s_b}\left\{[H_2O(0)] - \frac{2D\varphi_0}{\alpha R}\right\} \quad (25b)$$

Then, we have the solution for the time dependence of the H_3O^+ ions in the electrode region:

$$[H_3O^+(t)] = \frac{k_1 s_a}{k_2 s_b}\left\{[H_2O(0)] - \frac{2D\varphi_0}{\alpha R}\right\} + \frac{2k_1 s_a D\varphi_0}{\alpha R(k_2 s_b - \alpha)} e^{-\alpha t} \quad (26)$$

This solution does not hold when water lateral diffusion is absent, a condition for which the ratio D/α becomes fully undetermined being both D and α equal to zero.

Equation 26 can be further simplified, thus reducing the number of independent adjustable parameters in order to fit the experimental data, if we soundly assume that the reaction kinetics of protons extraction is faster than water diffusion. In this condition, the term $k_2 s_b$ would be much greater than α and equation 16 becomes:

$$[H_3O^+(t)] = \frac{k_1 s_a}{k_2 s_b}\left[[H_2O(0)] - \frac{2D\varphi_0(1 - e^{-\alpha t})}{\alpha R}\right] \quad (27a)$$

or, in terms of pH:

$$pH = -\log\{[H_3O^+](0) - [H_3O^+](\infty)e^{-\alpha t}\} \quad (27b)$$

where $pH(0) = -\log[H_3O^+(0)] = -\log\left\{\frac{k_1 s_a}{k_2 s_b}[H_2O(0)]\right\}$, is the acidity under the electrode surface at time zero and $pH(\infty)$, the asymptotic acidity value remaining under the electrode, given by:

$$pH(\infty) = -\log[H_3O^+(\infty)] = -\log\left\{[H_3O^+(0)] - \frac{2k_1 s_a D\varphi_0}{k_2 s_b \alpha R}\right\} \quad (28)$$

Eq. 27 can be more straightforwardly obtained from eq. 14 if it is assumed that reaction 11 reaches a stationary state in a very short time (seconds) such that $d[H_3O^+]/dt = 0$. In this case eq. 14 becomes:

$$[H_3O^+(t)] = \frac{k_1 s_a}{k_2 s_b}[H_2O(t)] \quad (29)$$

and eq. 27 is obtained by substituting in eq. 29, the value of $H_2O(t)$ given by eq.21.

Eq.27b predicts that, due to the diffusion of water across the paper, the pH value measured by a glass surface electrode, continously increases in time to reach an asimpthotic value, $[H_3O^+(\infty)]$, given by eq.28.

In order to derive an equation useful to reproduce the data obtained in absence of water lateral diffusion, we can directly integrate eq. 14. In this case, the time evolution of pH corresponds to the gradual proceeding of reaction 11 to its equilibrium state. The solution of eq. 14 can be simplified by introducing a sound approximation, i.e. that, at any time, $[H_2O(t)]$ is always much larger than $[H_3O^+(t)]$. This allows the substitution of $[H_2O(t)]$ with $[H_2O(0)]$. Eq. 14 can then be written as:

$$\frac{d}{dt}[H_3O^+] = c_1 - c_2[H_3O^+(t)]$$
$$c_1 = k_1 s_a [H_2O(0)] \qquad c_2 = k_2 s_b \tag{30}$$

Integration of eq. 30 leads to the following equation for the variation of pH with time:

$$pH = -\log\left\{[H_3O^+(0)]e^{-c_2 t} + [H_3O^+(\infty)]\left(1 - e^{-c_2 t}\right)\right\} \tag{31}$$

where, in this case, $[H_3O^+(\infty)] = \frac{k_1 s_a}{k_2 s_b}[H_2O(0)]$, while $[H_3O^+(0)]$ is the pH of pure water. It is interesting to notice that the asymptotic pH value obtained in the case of blocked diffusion is equal to the value of pH extrapolated at time zero when using eq. 27. This is not surprising when considering that eq. 27 is strictly valid if reaction 11 reaches the equilibrium in a time which is negligible with respect to the time of water diffusion.

Fitting of the experimental data

Surface pH data in the presence of water diffusion (TAPPI T 529 method)

The experimental data reported in Fig. 6.3 have been fitted by equation 17b, by varying the three fitting parameters pH(∞), pH(0) and α. The continuous lines in Fig 3 show the interpolation of the experimental data points while the obtained fitted parameters are reported in Tab.6.1. The first comment concerns the important difference between the values of pH(0) and pH(∞) which is of the range 0.3-0.5 pH units. In order to ensure reproducibility on pH data measured by the surface electrode method, it is not appropriate to consider values measured at times where the detected pH continues to evolve in time, since we cannot give any precise meaning to these measurements. Neither the use of the asymptotic pH value, pH(∞), seems to be the right choice since it depends on the value of the diffusion coefficient of water on the paper surface (eq. 28). In our opinion, the most appropriate pH value that should be used to define the paper acidity is the extrapolated one at time zero, i.e., pH(0). This value depends only on the equilibrium of the reaction between the acid sites of the paper with the water contacting the electrode surface, which generates the hydrogen ions.

Sample	pH(∞)	pH(0)	α (sec^{-1})
Black	5.31 (0.01)	4.79 (0.02)	0.046 (0.001)
Red	5.28 (0.01)	4.75 (0.04)	0.043 (0.001)
Blue	5.13 (0.01)	4.82 (0.03)	0.0180 (0.0007)
dark cian	5.14 (0.01)	4.88 (0.04)	0.018 (0.001)
Magenta	5.14 (0.01)	4.85 (0.03)	0.024 (0.001)

[a]Color according to the curves in Fig. 3

Table 5.1. Values of the parameters pH(∞), pH(0) and α obtained by fitting the data of Fig. 6.3 with equation 27b

It is worth to mention that the difference between $[H_3O^+(0)]$ and $[H_3O^+(\infty)]$ is proportional to the diffusion coefficient of water on the paper surface. This physical parameter is expected to be strongly dependent on paper porosity which, in turn, is expected to depend on the paper structural degradation. Paper ageing usually leads to an increase of the number of pores (micro holes) thus to

an increase of the water diffusion coefficient on paper. Our model allows the knowledge of the exponential time constant α which value is expected to increase with an increase of the diffusion coefficient and consequently, with an increase of the paper degradation. Therefore, we would expect that a useful correlation between this parameter and the conservation state of paper will be discovered, opening the way for new applications of the pH investigation by surface electrodes to study the conservation of paper historical artifacts.

On the light of the above considerations, we have a clear interpretation of the quite different trend of black and red curves measured on two points of page 24, with respect to that of blue, dark cyan, magenta curves related to measurements taken from page 187. Table 6.1 shows that the diversification between the two groups of data is not linked to their different acidity being the values of $[H_3O^+(0)]$ and $[H_3O^+(\infty)]$ almost equal within the experimental error. We like to underline that single measurements taken at time intervals ranging from zero sec up to 200 sec would have been interpreted in terms of a different acidity of page 24 with respect to that of page 187, without taking into consideration the real mechanism of the time evolution of the experimental data according to the model presented in this paper. The value of α is two times larger for pag. 24 than for pag. 187. This means that water diffuses faster on page 24 than in page 187, thus indicating that the paper has a different porosity for these two pages of the investigated book.

Surface pH data in the absence of water diffusion

The experimental data taken in absence of water diffusion (Fig 5.4) confirms the physical model above presented. In this case, the acidity, increases gradually with time to reach an asymptotic value. The trend is opposite to the one observed in the presence of water diffusion, due to the fact that only the gradual extraction of H_3O^+ by the water trapped in the region underlying the electrode is occurring. The parameters fitted by equation 20 are reported in Tab. 5.2. It can be seen that the values of pH(∞)obtained in absence of diffusion (Tab. 5.2) are very similar to pH(0) obtained when the diffusion mechanism is active (Tab. 5.1), as it is foreseen by the model developed in this paper.

Sample[a]	pH(∞)	pH(0)	c_2 (sec^{-1})
black	4.79 (0.01)	5.25(0.06)	0.063(0.006)
red	4.89 (0.01)	5.74(0.01)	0.026 (0.007)
blue	4.94 (0.01)	5.30(0.06)	0.056(0.004)
Suspension[b]	5.55 (0.01)	6.89 (0.02)	0.0020 (0.0003)

[a]Color according to the curves in Fig. 6.4. Data from Fig. 6.5

Table 5.2. *Values of the parameters pH(∞), pH(0) and c_2 obtained by fitting the data of Fig. 6.4 with equation 30*

Suspension pH data (TAPPI T 509 om-02 cold extraction method)

Finally we comment the results obtained by fitting the data reported in Fig. 5.5 measured according to the cold extraction method, when the paper/water weight ratio was 0.15. In this case, the value of pH(0) is practically the one of the pure milliQ water, while the value of $[H_3O^+(\infty)]$ is almost 0.6 unit higher than that measured in the experiment where the diffusion of water has been artificially prevented. This difference is simply due to the 4 times higher paper/water weight ratio used in the suspension method with respect to that used in the surface method. This corresponds to a dilution factor of 4 and accounts for the observed difference in the final pH of 0.6 unit.

5.4 Conclusions

This work has been motivated by the need to find an explanation of the continuous drifting of paper pH during the surface electrode measurement. A theoretical model which takes into account the diffusion of water through the paper under the electrode contact zone has been developed. This model has been tested by comparing experimental data taken according to the TAPPI T 529 procedure with data obtained when lateral water diffusion is avoid by confining the measurement zone in an appropriate way. The excellent agreement between the experimental time evolution of data and those calculated by means of the model leads to a clear identification of the time evolution of the dominant mechanisms influencing the time evolution of pH measures. One of the identified mechanism corresponds to the time evolution of the hydrogen ions concentration produced by the reaction between water and the acid sites of paper. The other mechanism is the related to the time

variation of the water concentration due to the diffusion of water molecules from the region lying beneath the surface electrode to surrounding region of the paper. Of course, the two mechanisms are interconnected, but it has been shown that, with a good approximation, they can be decoupled and very simple analytical solutions of the problems can be found. The model has been confirmed by fitting pH data obtained both in standard conditions and water diffusion prevented conditions. This paper finally suggests that, in order to have surface electrodes reproducible pH measurements on paper, the time evolution of the pH needs to be detected for a sufficiently long time intervals and that the extrapolated value at time zero needs to be calculated Furthermore, we suggest that the interpolation of data time evolution allows the knowledge of parameters that could be correlated to the conservation state of the paper.

References

Abdel-Maksoud, G., 2011. Analytical techniques used for the evaluation of a 19th century quranic manuscript conditions. Measurement, 44(9), 1606-1617.

Faubel, W., Staub, S., Simon, R., Heissler, S., Pataki, A., Banik, G., 2007. Non-destructive analysis for the investigation of decomposition phenomena of historical manuscripts and prints. Spectrochimica Acta Part B: Atomic Spectroscopy, 62(6), 669-676.

Launer, H. F. (1939). Determination of the pH Value of Papers. US Government Printing Office, Part of Journal of Research of the National Bureau of Standards 1939, 22, 553- 564

Strlic, M., Kolar, J., Kocar, D., Drnovsek, T., Selih, V. S., Susic, R., Pihlar, B., 2004. What is the pH of alkaline paper?. E-preservation science, (1), 35-47.

Strlič, M., Pihlar, B., Mauko, L., Kolar, J., Hočevar, S., Ogorevc, B., 2005. A new electrode for micro-determination of paper pH. Restaurator, 26(3), 159-171.

TAPPI Test Method T435 om-88, TAPPI Press, Atlanta, 1992.

TAPPI Test Method T509 om-88, TAPPI Press, Atlanta, 1992.

Part 3

New composite materials for cultural heritage restoration

In the third and final part of this thesis, we discuss two types of works. The first work (Chapter 6 "*New Fiber Composite Materials For Cultural Heritage Conservation*") is experimental and new fiber composite materials have been experimented and tested. We have obtained these new materials treating the surface of the cellulose fibers with a silane reactant used in the compounding internships to connect vegetables fibers to the other chemical components of the final composite materials. This work was presented at a conference (Heritage and Technology, XIII International Forum) and has also been patented. In the chapter 7 "" is presented the work that has been done during the internship abroad. The work is the use of new non-invasive diagnostic technologies for artworks. In particular they were examined by XRF (X Ray Fluorescence) and IR (Infra Red) spectrofotometer the wall paintings in the chapel located in the palace De La Salle site in Valletta, Malta.

Chapter 6

New Fiber Composite Materials For Cultural Heritage Conservation

New fiber composite materials are presented in this work. They have been obtained by treating the surface of the fibers with a silane reactant used in the compounding stage to connect vegetables and mineral fibers to the other chemical components of the final composite materials. The silane reactant links on the surface of the fiber forming strong covalent bonds through the Si atoms. The other end moiety of the silane reactant carries an ammine group which is able to bind to epoxides in a copolymerization process. In such a way the fiber themselves becomes part of polymer networks which have much better mechanical properties with respect to the composite materials obtained by simply dispersing the fibres into polymer matrices. The observed physical and mechanical proprieties of these fiber composites candidates them to have future interesting applications in the field of conservation of cultural heritage.

6.1 Introduction

A great interest has grown, in recent years, for eco-compatible materials which could be used in conservation and restoration of historical buildings and monuments. Several regional and national governmental institutions did reserve funds and intervention lines to promote the development and use of new materials, more safe for the environment.

On the other hand, the introduction of new materials in the field of cultural heritage restoration and conservation presents some peculiar difficulties. Not only the materials need to have good technical and mechanical properties, but must be respectful of the principles that have been promulgated in various restoration charts and reasserted in all sector debates.

Today the term bio-compatibility used with respect to building materials, is often associated with composites obtained from natural products such as wood and vegetable fibers most of which are

still in phase of development and testing. Among the main products appeared on the market, the following ones deserve particular interest with respect to building applications:

- Hemp bio-bricks, produced by combining the woody part (canapulo) of the hemp steam with lime water and appear to have a lover density with respect to mineral bricks, good mechanical properties, thermo-acustic insulation character, transpirability, optimal thermo-hygrometric equilibrium.
- Bricks recovered from paper fabric waste water are mixed with clay and finely extruded as bricks.

When conservation of historical monuments and buildings are taken into consideration research efforts need to be done to develop restoration product having some peculiar properties such as:

Good mechanical properties

• Low weight
• Durability
• Reversibility (easy to be removed if required)
• Well defined permeability to oxygen and humidity
• Long life
• Good stability with respect to biologic degradation

Composite materials where natural vegetable and mineral fibers are mixed with polymers are in principle good candidate to achieve the above mentioned properties. Chemical and Physical properties of composite materials can be in fact graduated by varying the nature of components, their percentage and the fabrication processes.

Researches on natural fibers/polymer composites, developed almost everywhere in industrialized countries, have shown that the simple addition of vegetable or mineral fibers to polymers do not leads to the improvement of the mechanical properties as requested specially from automotives industries (Lu et al., 2005a). It is now well understood that the failure of this approach is mainly linked to the hydrophilic nature of the natural fibers that lowers the compatibility with hydrophobic polymers largely used in automotive components, such as polypropylene (PPR) and polyethylene (PPE), polyurethanes and so on. Cellulose fibers contain indeed many hydroxyl groups (-OH) which strongly interact with water but are rejected by the hydrophobic surface of polymer giving a very poor adhesion at the interfaces (Lu et al., 2005a; 2005b).

Efforts have been made to overcome this problem mainly by using coupling agents to improve the compatibility and adhesion between polar wood fibers and non-polar polymer matrices both by coating the fibers by hydrophobic media and forming bridges of chemical bonds between the fibers and the polymer matrix (Lu et al., 2005b). Many examples of this strategy relate to the use of the maleic anhydrite and similar compounds to compatibilize natural fibers with polypropylene and

polyethylene. Other examples concern the use of silane compounds to increased the interfacial adhesion between fibers and polymer matrices.

Recently new types of vegetable fibers have been introduced in the scenario of natural fibers that can be conveniently used in combination with polymers to obtain improved composites (Chidichimo *et al*., 2015a; Danieli *et al.,* 2014; Chidichimo *et al*., 2015b; Chidichimo *et al.,* 2015c; Chidichimo *et al*., 2007; Cassano *et al.,* 2007; Cerchiara *et al.,* 2004). This new fibers are obtained from Spartium Junceum (SJ) plant: a vegetable which is endemic in Mediterranean countries. Here we present new polymer composites obtained from cellulose fibers extracted by Spartium Junceum (SJ), Portland cement (PC) and epoxy resin precursors. An innovative process of composite preparation has been developed. The vegetable fibers as well as the mineral cement particles, have been previously treated with 3-aminopropyltri-ethoxysilane, in order to link its silane moiety with the surface hydroxyls groups of both types of fibers, and leaving free reactive ammine terminal ends able to link the fibers with the epoxides precursor by covalent chemical bonds. The mechanical properties of these composites have been investigate. The particular valence of these composites in the framework of conservation and restoration of historical buildings is linked to the fact that the composites before the final curing is in a viscous plastic state that can be shaped as a plaster on the surface the surface that need to be restored, and can be shaped in any particular morphologic state.

6.2. Experimental

Vegetable fibres have been extracted from SJ plants by digesting the vegetable in a 5% by weight sodium idroxide solution, for half hour at a temperature of 80°C (Bartolo *et al.,* 2010). Cellulose fibers separate by simply washing the digested vegetable in fresh water. Fibers have been dried in an oven till constant weight at 80°C. SJ Fibers have been grinded by a RETSH-ZM 200 mill at dimension of short cylinders having a diameter of about 20 micrometers and a length of 120 micrometers. PC particles had an almost spherical shape with average diameter of 50 micrometers. Both these types of particles have been functionalized with the 3-aminopropyltri-ethoxysilane. This operation has been performed in a solvent free process. Cellulose and cement, mixed in the desired percentage, were inserted in an home-made reactor where they have been kept whirling stirred and humidified with nebulized water (10% of water with respect to the total weight of fibre components). 5% (w/w) of the functionalizing silane reactants (VTMS), was then added into the reactor as micrometer-sized droplets. The preliminary fibres humidification was required in order to

hydrolyze the silane ethoxy groups, next to the surface of the fibers were the water molecules were absorbed, according to the following 3 step reaction scheme:

1. Hydrolysis:

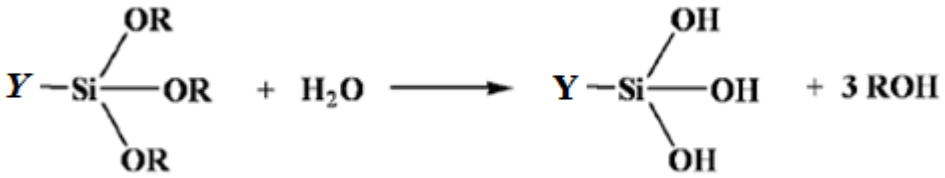

(8)

2. Condensation:

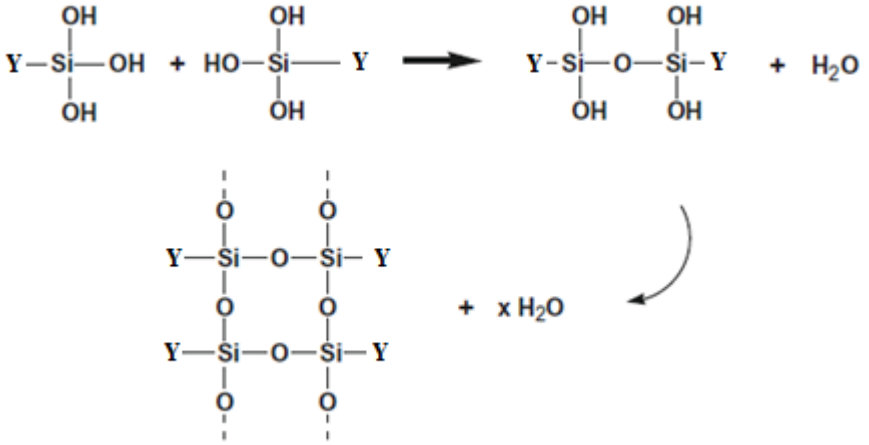

(9)

3. Dehydration with alcohol groups of the cellulose (*chemically grafting*) (Xie *et al.*, 2010):

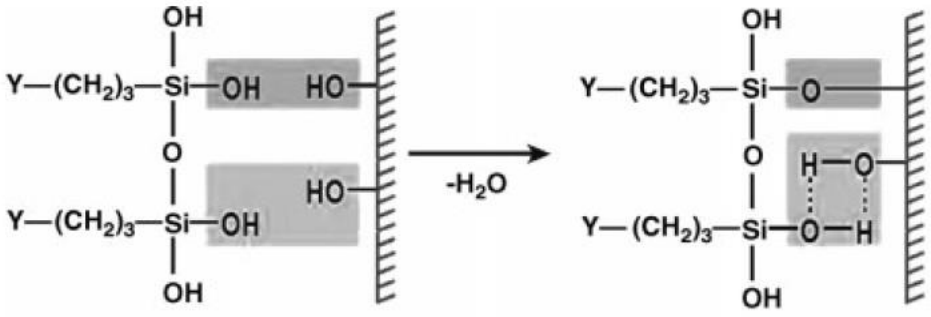

(10)

Following the reaction, the fiber will be linked to the VTMS as represented in Figure 4.1

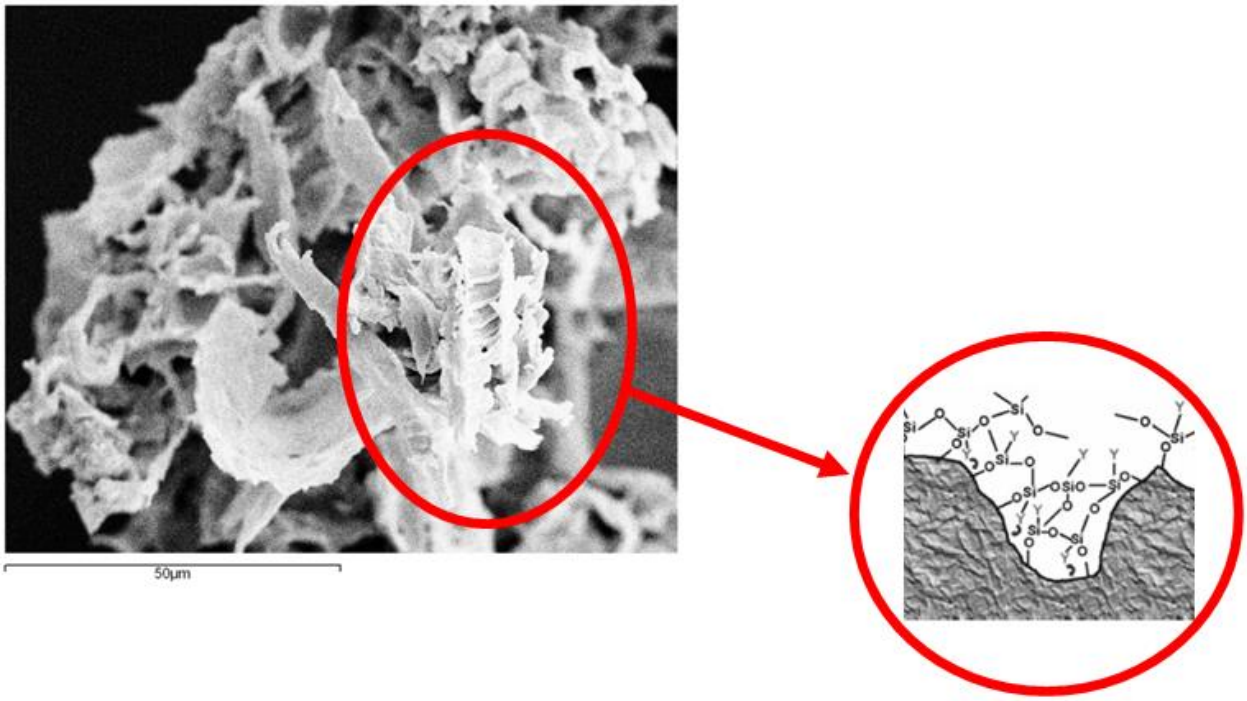

Figure 6.1- *Interaction beetween VTMS and the fiber (functionalization) and himself (polymerization).*

The Y group in the Chemical reactions and in the Fig.6.1 is the ammine group $–NH_2$. Fibers, functionalized according to the above reactions, were mixed, by an appropriate mixer, with two epoxy precursor: the Diglycydil ether of bisphenol A (DIGEBA) and the hardener diethylenetriammine (DETA) which were always used in the 2:1 proportion. The mixture was injected into a stamp and pressed to a pressure of 1.8 bars. Final curing of samples was achieved at 25 °C. The laboratory steps used to prepare the composite are summarized in Fig.4.2. Mechanical properties of the bio-materials were measured by using a universal testing machine (MTS Criterion s42) equipped with 5kN load cell and three point bending kit. In the bending tests, the load was applied with a rate of 50 mm/min. During the test the crosshead displacement Y and the applied load P were measured.

Figure 6.2 *A - vegetable(white) mineral fibers (dark) and mineral fibers; B and C - home made stamp*

To verify the correct functionalization, various types of analyzes have been performed.

SEM analysis

To verify the morphological structure of the cellulose with the VTMS, analysis by SEM were made. The analysis were permormed by a LEO 420. The samples were metallized all with gold and the analysis were performed under vacuum condition (10^{-6} torr) and at a current of the probe equal to 150 pA.

Three samples were analyzed. a cellulose non-functionalized (Fig.6.3A), one of the functionalised cellulose with 5% (w / w) of the VTMS (Fig.6.3B) and one with 10% (w / w) of the VTMS (Fig.6.3C)

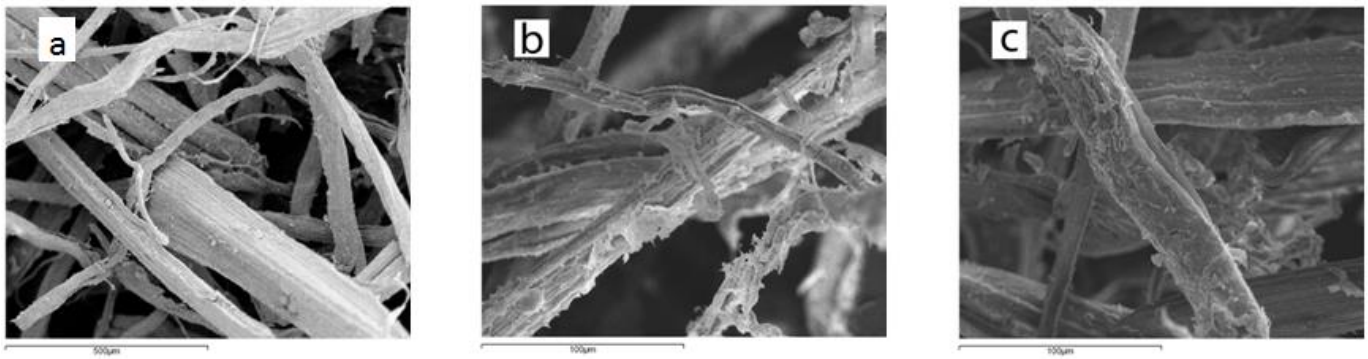

Figure 6.3 *Three samples analyzed. A) cellulose non-functionalized, B) cellulose functionalized with 5% (w / w) of the VTMS and C) cellulose functionalized with 10% (w / w) of the VTMS (Fig.6.3C)*

The samples show a clear polymerization in samples B and C on the surface of the cellulose.

IR analysis

To verify the presence of the silane functional groups, the analyzes were performed by a FT-IR spectrophotometer. Analyzes were carried out with the *Bruker Front Reflection Module A241D*.

The instrument has the following specifications:

- Spectral range: 375 - 5500 cm-1;
- Gold mirror for reference measurements;
- Sample spot diameter: 5mm (option 3mm);
- Sample spot distance from instrument front: 15mm

IR analysis has been reported in Fig. 6.4.

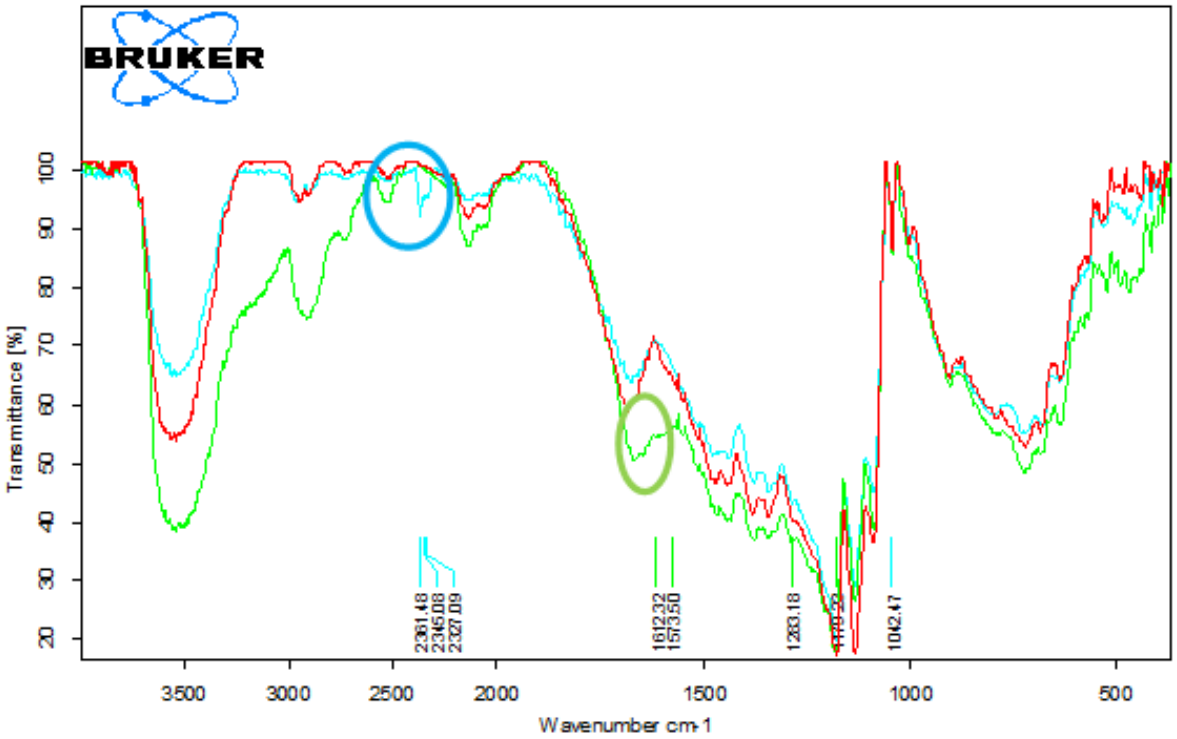

Figure 6.4. *The IR analysis. In red it is reported the no functionalized fiber. In blue, the spectrum of the functionalized fiber with VTMS 5 (w/w)). In green in the spectrum of the functionalized fiber with VTMS 10% (w/w)*

In the spectrum of Fig.6.4, are reported the analysis for a fiber sample not functionalized (in red), a fiber sample functionalized with VTMS (5% w / w) (in blue) and a fiber sample functionalized with VTMS were reported (10% w / w) (in green). Comparing with the literature data (Abidi et al., 2006), may be able to identify the hydrides of silane (region comprised between 2100-2400 cm^{-1}), the peaks belonging to trimethoxysilane (799, 1092, 1192 cm^{-1}) and also the siloxane (1080 cm^{-1}) as synthesized in Tab.6.1

Group	Structure	Wave number (cm^{-1})
Hydrides of Silane	$Si - H(-H_{2;} - H_3)$	2100-2400
Trimethoxysilane	$Si - OCH_3$	799, 1092, 1192
Siloxane	Si –O –Si	1080

Tab. 6.1 - *Wave numbers relative to the links of the VTMS with cellulose*

Furthermore, according to Abidi et al. (2006), the presence of additional peaks, located between 1650 and 1400cm^{-1} (highlighted in green in the Figure 6.4), indicating coordination between the OH groups of the cellulose with the VTMS.

6.3 Results and discussion

Table 6.2 summarizes the mechanical properties of the composites analysed, as a function of the composition of the various components of the mixture.

Sample	**SJ %**	**PC%**	**DIGEBA %**	**DETA)%**	**Mod El. E(MPa)**	**Flex. Strenght σ(MPa)**
1	60.00	/	26.66	13.33		
2	38.43	19.32	28.41	14,20	2424,83	24.69
3	29.12	29.11	28,23	14.12	8716,60	18.26
4	19.59	39.22	27.93	13.96	10583,65	23.26
5	9.91	49.53a	27.20	13.60	20273,27	72.99
6	/	61,05	26.00	13.00	15285.04	58.23

Tab. 6.2 *Composites formulation and their mechanical properties*

Data reported in Table 6.2 show that the mechanical properties of the polymer composites strongly depend on the composition of the precursor mixture. Interestingly, the elastic modulus and flexural strength increase as the concentration of functionalized SJ fiber decreases and that of the mineral particles increases. Nevertheless, composites containing only Portland cement, show worst mechanical properties with respect to the composites containing 10% of vegetable fibre, highlighting the significant role played by the vegetable fibre on the final properties of the composites.

Even if the data presented in this paper are preliminary, it can be stated that the combination of mineral and vegetable functionalized fibers, in polymer composites, leads to improved materials. Since these materials are obtained by fast curing fluid viscous precursor mixtures, their application in the context of restoration cultural heritage buildings, appears to be an open opportunity.

References

Abidi, N., Hequet, E., Tarimala, S., 2006. Functionalization of Cotton Fabric with Vinyltrimethoxysilane. Textile Research Journal, 77, 668-674

Cassano R. , Trombino S. , Bloise E. , Muzzalupo R. , Iemma F. , Chidichimo G. , Picci N. , 2007. New broom fiber (*Spartium Junceum L.)* derivatives: preparation and characterization". Journal of Agricultural and Food Chemistry, 14 (55), 9489-9495.

Cerchiara T., Chidichimo G., Ferraro R., Vuono D., 2009. Use Of Spanish Broome canvas: effect of enviromental conditions", J. Cultural Heritage

Cerchiara T., De Rose R., Santagada G., De Filpo G., Chidichimo G., 2004 . SpartiumJunceum retting by Clostridium Felsineum and analysis of fibre. Polymer Fibres, , Manchester (UK), 14-16 July 2004.

Chidichimo G., Alampi C., Cerchiara T., Gabriele B., Salerno G., Vetere M. , 2007. Physical chemical process for production of vegetable fibres. Depositario: Università della Calabria. World Patent, WO2007102184A2 2007.

Chidichimo, G. , Aloise, A., Chidichimo, A., Maltese, V., Beneduci, A. , Senatore, A., Dalena, F., Corace, G. , Gabriele, B., Bonifati, M., 2015c. Functionalised natural composites fibres and processes for their production; CS 102015000012480, 21/04/2015

Chidichimo, G., Aloise, A., De Rango, A., Venneri, M., Pingitore, G., Esposito, G., 2015b. Compositi di vermene ginestre e processi per la loro realizzazione. Italian Patent, N° 102015000007277, 02, 03, 2015.

Chidichimo, G.,Aloise, A., Beneduci, A., De Rango, A., Pingitore, G., Furgiuele, F., Valentino, P., Polyurethanes reinforced with Spartium Junceum fibers. Polymer Composites,37 (10), 3042-3049 .

Danieli, G., Chidichimo, G., Greco, P.,F., Nudo , P., Aloise, A., De Rango, A., 2014 Impianto automatizzato per l'estrazione di fibre vegetali da piante. Cs 2014 A00002, 26, 06, 2014.

Gabriele, B. , Cerchiara, T. , Salerno G. , Chidichimo, G. , Vetere, M. , Alampi, C. , Gallucci M.,C., Conidi, C. , Cassano, A. , 2010. A new physical-chemical process for the efficient

production of cellulose fibers from Spanish broom (Spartiumjunceum L.). Bioresource Technology, 101 (2), 724-729.

John Z Lu, J.,Z., Wu, Q., Negulescu, I.,I., 2005b. Wood-Fiber/High-Density-Polyethylene Composites: Coupling Agent Performance,. Journal of Applied Polymer Science, 96, 93–102.

Lu, J.Z., Wu, Q., Harold, S.,M., 2005a. Chemical coupling in wood fibre and polymer composites: a review of coupling agents and treatments. Wood and Fibre Science 2000, 32 (1), 88 – 104.

Xie,Y., Hill, C.,A.,S., Xiao, V., Militz,H., Mai,C., 2010. Silane coupling agents used for natural fiber/polymer composites: A review. Composites, 41, 806–819.

Acknowledgements

Queste brevi righe non possono sintetizzare i sinceri ringraziamenti che vorrei porgere a tutti quelli che mi hanno accompagnato in questo percorso.

Non me ne vogliano tutti i miei fratelli che non verranno citati, ma i miei ringraziamenti sono rivolti a chi più di tutti ha contribuito affinché questo traguardo potesse essere raggiunto.

Ringrazio innanzitutto “Nat” per le cose incalcolabili che fa ogni giorno.

Ovviamente un particolare ringraziamento ai miei genitori per la costante fiducia che hanno riposto in me.

Vorrei ringraziare la dott.ssa Capparelli che è stata una luce nei labirinti burocratici nei quali tendo a orientarmi veramente male.

Ma più di tutti ringrazio il Prof. Giuseppe Chidichimo e il Prof. Angelo Basile sempre più mentori sia di Vita sia di Scienza. Vi devo molto.